Monthly Notices
of the
ROYAL ASTRONOMICAL SOCIETY

MNRAS **434,** 1220–1238 (2013) doi:10.1093/mnras/stt1080
Advance Access publication 2013 July 15

A detailed census of variable stars in the globular cluster NGC 6333 (M9) from CCD differential photometry⋆

A. Arellano Ferro,[1]† D. M. Bramich,[2] R. Figuera Jaimes,[2,3] Sunetra Giridhar,[4] N. Kains,[2] K. Kuppuswamy,[4] U. G. Jørgensen,[5,6] K. A. Alsubai,[7] J. M. Andersen,[8,6] V. Bozza,[9,10] P. Browne,[3] S. Calchi Novati,[9,11] Y. Damerdji,[12] C. Diehl,[13,14] M. Dominik,[3] S. Dreizler,[15] A. Elyiv,[12,16] E. Giannini,[13] K. Harpsøe,[5,6] F. V. Hessman,[15] T. C. Hinse,[17,5] M. Hundertmark,[3] D. Juncher,[5,6] E. Kerins,[18] H. Korhonen,[5,6] C. Liebig,[3] L. Mancini,[19] M. Mathiasen,[5] M. T. Penny,[20] M. Rabus,[21] S. Rahvar,[22,23] D. Ricci,[12,24] G. Scarpetta,[9,25] J. Skottfelt,[5,6] C. Snodgrass,[26] J. Southworth,[27] J. Surdej,[12] J. Tregloan-Reed,[27] C. Vilela[27] and O. Wertz[12] (The MiNDSTEp consortium)

[1]*Instituto de Astronomía, Universidad Nacional Autónoma de México, Ciudad Universitaria CP 04510, Mexico*
[2]*European Southern Observatory, Karl-Schwarzschild-Straβe 2, D-85748 Garching bei München, Germany*
[3]*SUPA, School of Physics and Astronomy, University of St. Andrews, North Haugh, St Andrews KY16 9SS, UK*
[4]*Indian Institute of Astrophysics, Koramangala 560034, Bangalore, India*
[5]*Niels Bohr Institute, University of Copenhagen, Juliane Maries vej 30, DK-2100 Copenhagen, Denmark*
[6]*Centre for Star and Planet Formation, Geological Museum, Øster Voldgade 5, DK-1350 Copenhagen, Denmark*
[7]*Qatar Foundation, PO Box 5825, Doha, Qatar*
[8]*Department of Astronomy, Boston University, 725 Commonwealth Ave, Boston, MA 02215, USA*
[9]*Dipartimento di Fisica 'E.R Caianiello', Universit di Salerno, Via Ponte Don Melillo, I-84084 Fisciano, Italy*
[10]*Istituto Nazionale di Fisica Nucleare, Sezione di Napoli, Italy*
[11]*Istituto Internazionale per gli Alti Studi Scientifici (IIASS), Vietri Sul Mare (SA), Italy*
[12]*Institut d'Astrophysique et de Géophysique, Université de Liège, Allée du 6 Août 17, Sart Tilman, Bât. B5c, B-4000 Liège, Belgium*
[13]*Astronomisches Rechen-Institut, Zentrum für Astronomie der Universität Heidelberg (ZAH), Mönchhofstr. 12-14, D-69120 Heidelberg, Germany*
[14]*Hamburger Sternwarte, Universität Hamburg, Gojenbergsweg 112, D-21029 Hamburg, Germany*
[15]*Institut für Astrophysik, Georg-August-Universität, Friedrich-Hund-Platz 1, D-37077 Göttingen, Germany*
[16]*Main Astronomical Observatory, Academy of Sciences of Ukraine, vul. Akademika Zabolotnoho 27, 03680 Kyiv, Ukraine*
[17]*Korea Astronomy and Space Science Institute, Daejeon 305-348, Korea*
[18]*Jodrell Bank Centre for Astrophysics, University of Manchester, Oxford Road, Manchester M13 9PL, UK*
[19]*Max Planck Institute for Astronomy, Königstuhl 17, D-69117 Heidelberg, Germany*
[20]*Department of Astronomy, Ohio State University, 140 West 18th Avenue, Columbus, OH 43210, USA*
[21]*Instituto de Astrofísica, Facultad de Física, Pontificia Universidad Católica de Chile, Av. Vicuña Mackenna 4860, 7820436 Macul, Santiago, Chile*
[22]*Department of Physics, Sharif University of Technology, PO Box 11155–9161, Tehran, Iran*
[23]*Perimeter Institute for Theoretical Physics, 31 Caroline St. N., Waterloo ON N2L 2Y5, Canada*
[24]*Instituto de Astronomía - UNAM, Km 103 Carretera Tijuana Ensenada, 422860 Ensenada (Baja Cfa), Mexico*
[25]*INFN, Gruppo Collegato di Salerno, Sezione di Napoli, Italy*
[26]*Max Planck Institute for Solar System Research, Max-Planck-Str. 2, D-37191 Katlenburg-Lindau, Germany*
[27]*Astrophysics Group, Keele University, Staffordshire ST5 5BG, UK*

Accepted 2013 June 13. Received 2013 June 9; in original form 2013 May 19

ABSTRACT

We report CCD *V* and *I* time series photometry of the globular cluster NGC 6333 (M9). The technique of difference image analysis has been used, which enables photometric precision better than 0.05 mag for stars brighter than $V \sim 19.0$ mag, even in the crowded central regions of the cluster. The high photometric precision has resulted in the discovery of two

⋆Based on observations collected with the 2.0 m telescope at the Indian Astrophysical Observatory, Hanle, India, and with the Danish 1.54 m telescope at the ESO La Silla Observatory in Chile.

† E-mail: armando@astro.unam.mx

new RRc stars, three eclipsing binaries, seven long-term variables and one field RRab star behind the cluster. A detailed identification chart and equatorial coordinates are given for all the variable stars in the field of our images of the cluster. Our data together with the literature V-data obtained in 1994 and 1995 allowed us to refine considerably the periods for all RR Lyrae stars. The nature of the new variables is discussed. We argue that variable V12 is a cluster member and an Anomalous Cepheid. Secular period variations, double-mode pulsations and/or the Blazhko-like modulations in some RRc variables are addressed. Through the light-curve Fourier decomposition of 12 RR Lyrae stars we have calculated a mean metallicity of $[\mathrm{Fe/H}]_{\mathrm{ZW}} = -1.70 \pm 0.01$(statistical) $\pm$ 0.14(systematic) or $[\mathrm{Fe/H}]_{\mathrm{UVES}} = -1.67 \pm 0.01$(statistical) $\pm$ 0.19(systematic). Absolute magnitudes, radii and masses are also estimated for the RR Lyrae stars. A detailed search for SX Phe stars in the Blue Straggler region was conducted but none were discovered. If SX Phe exist in the cluster then their amplitudes must be smaller than the detection limit of our photometry. The colour–magnitude diagram has been corrected for heavy differential reddening using the detailed extinction map of the cluster of Alonso-García et al. This has allowed us to set the mean cluster distance from two independent estimates; from the RRab and RRc absolute magnitudes, we find 8.04 ± 0.19 and 7.88 ± 0.30 kpc, respectively.

Key words: stars: fundamental parameters – globular clusters: individual: NGC 6333 – stars: variables: general – stars: variables: RR Lyrae.

1 INTRODUCTION

In the last thirty years, the variable stars in the globular cluster NGC 6333 (M9 or C1716−184 in the IAU nomenclature) ($\alpha = 17^{\mathrm{h}}19^{\mathrm{m}}11\overset{\mathrm{s}}{.}8$, $\delta = -18^{\circ}30'58\overset{''}{.}5$, J2000; $l = 5\overset{\circ}{.}54$, $b = +10\overset{\circ}{.}71$) have been the subject of some analyses based on photographic and CCD time series photometry (Clement, Ip & Robert 1984; Clement & Walker 1991; Clement & Shelton 1996, 1999). The 2012 update for NGC 6333 in the Clement et al. (2001) Catalogue of Variable Stars in Globular Clusters (CVSGC) lists 21 known variable stars; nine RRab, nine RRc, one long period variable (V8), one Pop II Cepheid (V12) and one eclipsing binary (V21). This makes the cluster attractive for a Fourier decomposition analysis of the RR Lyrae star light curves with the aim of calculating their physical parameters from semi-empirical calibrations. Furthermore, this cluster has a crowded central region where it is difficult to perform conventional point spread function (PSF) fitting photometry. The application of difference image analysis (DIA) to image data for this cluster for the first time therefore opens up the possibility of new variable star discoveries.

Recently our team has performed CCD photometry of several globular clusters by employing the DIA technique to produce precise time series photometry of individual stars down to $V \sim 19.5$ mag. The DIA photometry has proven to be a very useful tool in obtaining high-quality light curves of known variables, and for discovering and classifying new variables (e.g. Arellano Ferro et al. 2011; Bramich et al. 2011; Kains et al. 2012; Figuera Jaimes et al. 2013; and references therein), where previous CCD photometric studies have not detected stellar variability, particularly in the crowded central regions of the clusters. Thus, in this paper we report the analysis of new time series photometry of NGC 6333 in the V and I filters. In Section 2, we describe the observations and data reductions. In Section 3, the problem of the differential reddening in the cluster field of view (FOV) is addressed and the approach we used to correct it is described. Section 4 contains a detailed discussion on the approach to the identification of new variables and their classification. In Section 5, we apply Fourier light-curve decomposition to some of the RR Lyrae stars and calculate their metallicity and absolute magnitude. Given the differential reddening correction, the accuracy in the cluster distance determination is highlighted. In Section 6, we discuss the A_V - log P relation for the RR Lyrae stars and the Oosterhoff type of the cluster. In Section 7, we summarize our results.

2 OBSERVATIONS AND REDUCTIONS

2.1 Observations

The observations employed in this work were performed using the Johnson V and I filters on 15 nights during 2010–2012 at two different observatories. The 2.0 m telescope of the Indian Astronomical Observatory (IAO), Hanle, India, located at 4500 m above sea level, was used to obtain 212 and 171 epochs in the V and I filters, respectively. The detector was a Thompson CCD of 2048 × 2048 pixels with a pixel scale of 0.296 arcsec pixel^{-1} translating to an FOV of approximately 10.1 × 10.1 arcmin^2. Also, the Danish Faint Object Spectrograph and Camera (DFOSC) at the Danish 1.54 m telescope at La Silla, Chile, was used to collect 118 epochs in the V filter. DFOSC has a 2147 × 2101 pixel Loral CCD with a pixel scale of 0.396 arcsec pixel^{-1} and an FOV of ∼14.2 × 13.9 arcmin^2.

The log of observations is shown in Table 1 where the dates, site, number of frames, exposure times and average nightly seeing are recorded. A total of 330 epochs in the V filter and 171 in the I filter spanning just over two years are included in this study.

2.2 Difference image analysis

We employed the technique of DIA to extract high-precision photometry for all of the point sources in the images of NGC 6333 and we used the DANDIA[1] pipeline for the data reduction process

[1] DANDIA is built from the DanIDL library of IDL routines available at http://www.danidl.co.uk.

Table 1. The distribution of observations of NGC 6333 for each filter, where the columns N_V and N_I represent the number of images taken with the V and I filters, respectively. We also provide the exposure time, or range of exposure times, employed during each night for each filter in the columns t_V and t_I and the average seeing in the last column.

Date	Telescope	N_V	t_V (s)	N_I	t_I (s)	Avg seeing (arcsec)
20100506	2.0 m IAO, Hanle, India	29	180–250	26	40–60	2.2
20110412	2.0 m IAO, Hanle, India	4	75–125	5	10–60	1.5
20110413	2.0 m IAO, Hanle, India	11	70	11	8–10	1.4
20110414	2.0 m IAO, Hanle, India	14	70	14	10	1.4
20110610	2.0 m IAO, Hanle, India	13	70–100	13	10–15	1.7
20110611	2.0 m IAO, Hanle, India	3	200–250	3	10–40	2.8
20110805	2.0 m IAO, Hanle, India	13	100–200	13	15–50	1.8
20110806	2.0 m IAO, Hanle, India	6	90–100	6	12–15	1.9
20120515	2.0 m IAO, Hanle, India	3	20–40	3	7–20	1.9
20120516	2.0 m IAO, Hanle, India	23	10–35	24	4–35	1.8
20120628	2.0 m IAO, Hanle, India	52	20–60	53	3–15	2.2
20120629	2.0 m IAO, Hanle, India	41	40–100	–	–	2.7
20120822	1.54 m Danish, La Silla, Chile	28	100–180	–	–	3.1
20120824	1.54m Danish, La Silla, Chile	39	50–100	–	–	1.8
20120826	1.54m Danish, La Silla, Chile	51	50	–	–	1.0
Total:		330		171		

(Bramich et al. 2013) which includes an algorithm that models the convolution kernel matching the PSF of a pair of images of the same field as a discrete pixel array (Bramich 2008).

The DANDIA pipeline performs standard overscan bias level and flat-field corrections of the raw images, and creates a reference image for each filter by stacking a set of registered best seeing calibrated images. For the La Silla image data, which are slightly undersampled in the best seeing images, it was necessary to pre-blur any images with a seeing of less than 3 pixel to force a full width at half-maximum (FWHM) of the PSF of at least 3 pixel. This is because undersampling can cause problems in determining the kernel solution matching the PSFs between images.

We constructed three reference images, one in the V filter for each telescope and one in I for the Hanle data. For each of these reference images, 5, 10 and 6 calibrated images were stacked with total exposure times of 350, 500 and 50 s in the V (Hanle), V (La Silla) and I (Hanle) filters, respectively, with PSF FWHMs of ∼4.3, ∼3.2 and ∼3.5 pixel, respectively. In each reference image, we measured the fluxes (referred to as reference fluxes) and positions of all PSF-like objects (stars) by extracting a spatially variable (with a third-degree polynomial) empirical PSF from the image and fitting this PSF to each detected object. The detected stars in each image in the time series were matched with those detected in the corresponding reference image, and a linear transformation was derived which was used to register each image with the reference image.

For each filter, a sequence of difference images was created by subtracting the relevant reference image, convolved with an appropriate spatially variable kernel, from each registered image. The spatially variable convolution kernel for each registered image was determined using bilinear interpolation of a set of kernels that were derived for a uniform 6 × 6 grid of subregions across the image.

The differential fluxes for each star detected in the reference image were measured on each difference image. Light curves for each star were constructed by calculating the total flux $f_{\rm tot}(t)$ in ADU/s at each epoch t from:

$$f_{\rm tot}(t) = f_{\rm ref} + \frac{f_{\rm diff}(t)}{p(t)}, \quad (1)$$

where $f_{\rm ref}$ is the reference flux (ADU/s), $f_{\rm diff}(t)$ is the differential flux (ADU/s) and $p(t)$ is the photometric scale factor (the integral of the kernel solution). Conversion to instrumental magnitudes was achieved using

$$m_{\rm ins}(t) = 25.0 - 2.5 \log [f_{\rm tot}(t)], \quad (2)$$

where $m_{\rm ins}(t)$ is the instrumental magnitude of the star at time t. Uncertainties were propagated in the correct analytical fashion.

The above procedure and its caveats have been described in detail in Bramich et al. (2011) and the interested reader is referred there for the relevant details.

2.3 Photometric calibrations

2.3.1 Relative

All photometric data suffer from systematic errors to some level. Sometimes they may be severe enough to be mistaken for bona fide variability in light curves (e.g. Safonova & Stalin 2011). However, multiple observations of a set of objects at different epochs, such as time series photometry, may be used to investigate, and possibly correct, these systematic errors (see for example Honeycutt 1992). This process is a relative self-calibration of the photometry, which is being performed as a standard post-processing step for large-scale surveys (e.g. Padmanabhan et al. 2008; Regnault et al. 2009; etc.).

We apply the methodology developed in Bramich & Freudling (2012) to solve for the magnitude offsets Z_k that should be applied to each photometric measurement from the image k. In terms of DIA, this translates into a correction (to first order) for the systematic error introduced into the photometry from an image due to an error in the fitted value of the photometric scale factor p. We found that for Hanle images in either filter the magnitude offsets that we derive are of the order of ∼10 mmag with a handful of worse cases reaching ∼30 mmag. For the La Silla data, the magnitude offsets that we derive are of the order of ∼1–5 mmag. Applying these magnitude offsets to our DIA photometry notably improves the light-curve quality, especially for the brighter stars.

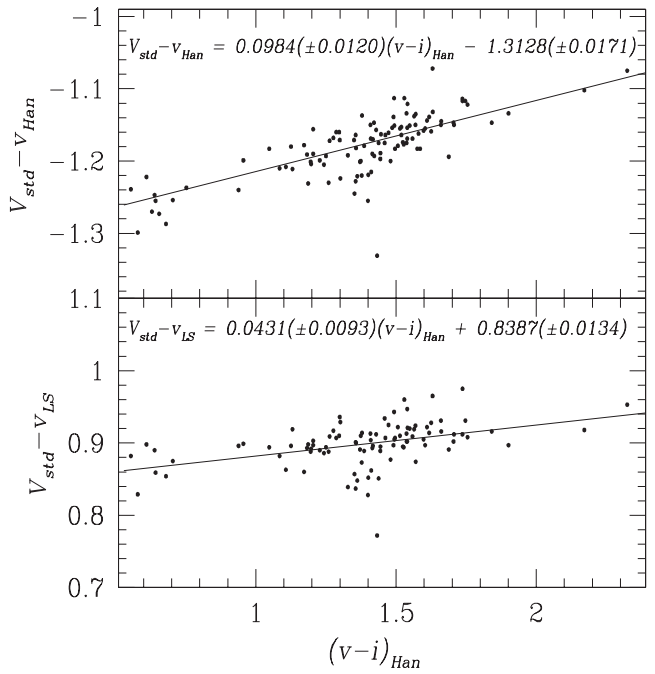

Figure 1. Transformation relations between the instrumental and the standard photometric systems using a set of standard stars in the field of NGC 6333 provided by Peter Stetson. Top and bottom panels correspond to the observations from Hanle and La Silla, respectively. The lack of *I*-band standards forced us to leave the Hanle *I* data in the instrumental system. The *V* observations from La Silla have been fitted with the Hanle colour $(v-i)_{\rm Han}$ to reveal the colour dependence. See Section 2.3.2 for a discussion.

2.3.2 Absolute

Standard stars in the field of NGC 6333 are not included in the online collection of Peter Stetson.[2] However, Professor Stetson has kindly provided us with a set of preliminary standard stars which we have used to transform instrumental *v* magnitudes into the standard *V* system. The lack of equivalent values in the *I* filter forced us to leave our observations for this filter in the instrumental system.

The standard minus the instrumental magnitudes show mild dependences on the colour, as can be seen in Fig. 1. The transformations are of the form

$$V_{\rm std} = v_{\rm Han} + 0.0984(\pm0.0120)(v-i)_{\rm Han} - 1.3128(\pm0.0171), \quad (3)$$

$$V_{\rm std} = v_{\rm LS} + 0.0431(\pm0.0093)(v-i)_{\rm Han} + 0.8387(\pm0.0134). \quad (4)$$

Due to the lack of observations in the *I* band for La Silla, equation (4) was fit using the Hanle colour $(v-i)_{\rm Han}$. For the La Silla data, we have adopted $(v-i)_{\rm Han} = 0.8$ mag which corresponds approximately to the centre of RR Lyrae horizontal branch (HB), hence

$$V_{\rm std} = v_{\rm LS} + 0.8731(\pm0.0163), \quad (5)$$

which we have used to transform the instrumental into the standard magnitudes for La Silla. Given the instrumental colour range of RR Lyrae stars, 0.60–1.0, this practice produces standard *V* magnitudes consistent with the zero-point uncertainties of the above equations. For much redder variables, like those at the tip of the red giant branch (RGB), the standard *V* magnitudes for the La Silla data may be off by as much as 0.025 mag. Due to saturation in the *I*-band images, variable V29 has no $v-i$ value and we have also adopted $(v-i)_{\rm Han} = 0.8$ to calculate its standard *V* magnitudes.

All of our *Vi* photometry for the variable stars in the field of the La Silla images of NGC 6333 is provided in Table 2. Only a small portion of this table is given in the printed version of this paper while the full table is available in electronic form.

Fig. 2 shows the rms magnitude deviation in our *V* and *i* light curves, after the relative photometric calibration of Section 2.3.1, as a function of mean magnitude. We achieve rms scatter at the bright end of ∼10–20 mmag in both the *V* and *I* filters for the Hanle data, while we achieve an even better rms for all magnitudes for the La Silla data with an rms at the bright end of ∼3–5 mmag. We believe that the La Silla data, which come from the smaller of the two telescopes, performed significantly better in terms of S/N due to a combination of better seeing for the majority of images and more stable flat-fielding.

2.4 Astrometry

A linear astrometric solution was derived for the *V*-filter reference image from La Silla (which has the larger FOV) by matching ∼600 hand-picked stars with the Third US Naval Observatory CCD Astrograph Catalog (UCAC3; Zacharias et al. 2010) using a field overlay in the image display tool GAIA (Draper 2000). We achieved a radial rms scatter in the residuals of ∼0.3 arcsec. The astrometric fit was then used to calculate the J2000.0 celestial coordinates for all of the confirmed variables in our FOV (see Table 3). The coordinates correspond to the epoch of the *V* reference image from La Silla, which pertains to the heliocentric Julian day 245 6166.51 d.

3 REDDENING

NGC 6333 is known to have differential reddening (Clement et al. 1984) with a heavily obscuring cloud to the SW of the cluster which is evident in the cluster images. Hence, without a proper correction for the differential reddening effects it would be difficult to tell how much of the dispersion in the position of the RR Lyrae stars in the colour–magnitude diagram (CMD) is due to reddening and how much is due to physical and evolutionary effects. The large dispersion in the HB and RGB in the uncorrected CMD shown in the left-hand panel of Fig. 3 is evident, and it is particularly visible in the distribution of the RR Lyrae stars.

Foreground reddening estimates for NGC 6333 can be found in the literature, e.g. $E(B-V) = 0.34$ mag (Zinn 1985); 0.32–0.37 mag (Reed, Hesser & Shawl 1988); 0.38 mag (Harris 1996, 2010 edition).

To correct for the differential reddening, we have taken advantage of the detailed reddening maps calculated by Alonso-García et al. (2012) for a group of globular clusters in the inner Galaxy including NGC 6333. In the map for this cluster, differential reddenings are presented for a grid of 27 668 coordinates within ∼11 arcmin centred in the field of the cluster and with a spatial resolution of ∼3.6 arcsec. For each star in our Hanle reference images, we averaged the differential reddenings for the four neighbouring values in the grid and follow Alonso-García et al. in using the absolute extinction zero-point of $E(B-V) = 0.43$ mag, estimated by comparing with the map of Schlegel, Finkbeiner & Davis (1998) to obtain a reddening. Then, we corrected our *V* and *i* magnitudes for each star by adopting a normal extinction $A_V = 3.1E(B-V)$ and the ratio $A_I/A_V = 0.479$ (Cardelli, Clayton & Mathis 1989) from which

[2] http://www3.cadc-ccda.hia-iha.nrc-cnrc.gc.ca/community/STETSON/standards

Table 2. Time series V and i photometry for all the confirmed variables in our FOV. The telescope employed is coded in column 2 (2.0H = 2 m telescope in Hanle; 1.5LS = 1.54 m telescope in La Silla). The standard $M_{\rm std}$ and instrumental $m_{\rm ins}$ magnitudes are listed in columns 5 and 6, respectively, corresponding to the variable star in column 1. Filter and epoch of mid-exposure are listed in columns 3 and 4, respectively. The uncertainty on $m_{\rm ins}$ is listed in column 7, which also corresponds to the uncertainty on $M_{\rm std}$. For completeness, we also list the quantities $f_{\rm ref}$, $f_{\rm diff}$ and p from equation (1) in columns 8, 10 and 12, along with the uncertainties $\sigma_{\rm ref}$ and $\sigma_{\rm diff}$ in columns 9 and 11. This is an extract from the full table, which is available with the electronic version of the article (see the supporting information).

Variable star ID	Telescope	Filter	HJD (d)	$M_{\rm std}$ (mag)	$m_{\rm ins}$ (mag)	σ_m (mag)	$f_{\rm ref}$ (ADU s^{-1})	$\sigma_{\rm ref}$ (ADU s^{-1})	$f_{\rm diff}$ (ADU s^{-1})	$\sigma_{\rm diff}$ (ADU s^{-1})	p
V1	2.0H	V	245 5323.252 94	16.512	17.735	0.004	843.914	3.864	−28.802	2.353	0.7536
V1	2.0H	V	245 5323.266 83	16.520	17.742	0.004	843.914	3.864	−34.345	2.301	0.7816
⋮	⋮	⋮	⋮	⋮	⋮	⋮	⋮	⋮	⋮	⋮	
V1	2.0H	I	245 5323.271 16	0.000	16.632	0.007	2073.761	12.792	+115.682	10.584	0.7681
V1	2.0H	I	245 5323.297 22	0.000	16.636	0.006	2073.761	12.792	+110.797	10.198	0.7825
⋮	⋮	⋮	⋮	⋮	⋮	⋮	⋮	⋮	⋮	⋮	
V1	1.5LS	V	245 6162.621 83	16.488	15.615	0.004	9079.038	11.294	−3191.886	21.994	0.9373
V1	1.5LS	V	245 6162.623 29	16.486	15.613	0.004	9079.038	11.294	−3193.007	21.104	0.9406

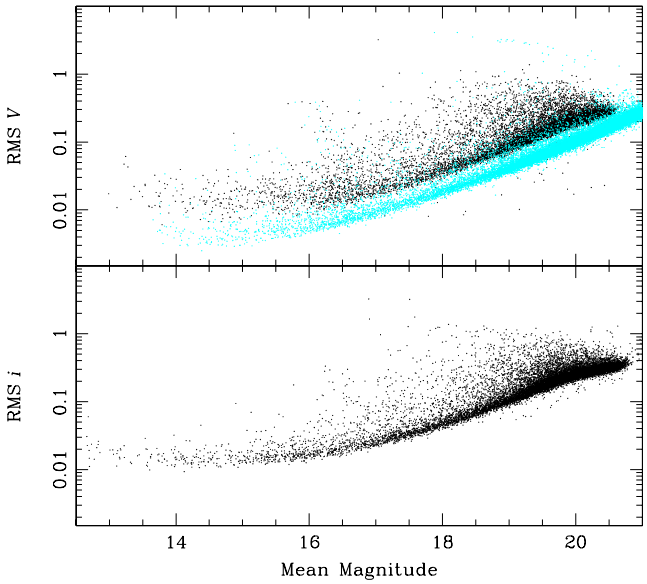

Figure 2. The rms magnitude deviations as a function of magnitude. The upper panel corresponds to the V light curves from Hanle (black dots, 12 519 stars) and La Silla (cyan dots, 21 143 stars). The lower panel corresponds to the i light curves from Hanle (15 524 stars).

$E(V-I)/E(B-V) = 1.616$ follows. The resulting corrected CMD is shown in the right-hand panel of Fig. 3. The RR Lyrae stars have been plotted using their intensity-weighted magnitudes calculated by fitting equation (9) (A_o) to their light curves.

Individual reddenings for the RRab stars may also be calculated from their colour near minimum light. The method, originally proposed by Sturch (1966), has been further investigated by Blanco (1992), Mateo et al. (1995), Guldenschuh et al. (2005) and Kunder, Chaboyer & Layden (2010). Guldenschuh et al. (2005) concluded that for RRab stars the intrinsic colour between phases 0.5 and 0.8 is $(V-I)_o^{\phi(0.5-0.8)} = 0.58 \pm 0.02$ mag. For the RRab stars in NGC 6333 we have calculated the mean $V-i$ colour curves as the difference between the Fourier fits from equation (9) for the standard V and instrumental i light curves. A plot of the colour curves in the 0.5–0.8 phase interval is shown for each star in the top panel of Fig. 4. The different mean levels of the $(V-i)^{\phi(0.5-0.8)}$ curves are due to the differential reddening affecting the cluster. Then, relative to V1, $\Delta E(V-I)^{\phi(0.5-0.8)} = (V-i)_{var}^{\phi(0.5-0.8)} - (V-i)_{V1}^{\phi(0.5-0.8)}$ which in turn is used to calculate $\Delta E(B-V)^{\phi(0.5-0.8)} = \Delta E(V-I)^{\phi(0.5-0.8)}/1.616$ for each RRab star. These colour excesses can be compared with the independent values obtained from the reddening map $E(B-V)^{\rm map}$. In the bottom panel of Fig. 4, we show the comparison of $\Delta E(B-V)^{\phi(0.5-0.8)}$ versus $\Delta E(B-V)^{\rm map} = E(B-V)_{\rm var}^{\rm map} - E(B-V)_{V1}^{\rm map}$. The result should be a linear relation with unit gradient. Clearly the differential reddening in the Alonso-Garcia et al. maps and the estimated ones from the RR Lyrae stars $V-i$ curves in the 0.5–0.8 phase range are, within the uncertainties, consistent.

The final adopted values of $E(B-V)$ for all of the RR Lyrae stars are those from the Alonso-García et al. (2012) reddening map and they are listed in column 12 of Table 4.

4 VARIABLE STARS IN NGC 6333

The globular cluster NGC 6333 has not been explored by many investigators in search of variable stars. The first variable star was discovered by Shapley (1916). 35 years passed until 12 more variable stars were discovered by Sawyer (1951) as part of a photographic survey. Sawyer (1951) also measured the periods of the 13 known variables and labelled them V1–V13. The variable stars in NGC 6333 were not studied again until Christine Clement and collaborators started to work on the cluster another 35 years later publishing four papers of interest. One of the papers (Clement & Shelton 1996) reports on a search for new variables using CCD data which was successful in yielding eight new detections (V14–V21) and extracting a light curve for V11 for the first time. The other papers in the Clement series (Clement et al. 1984; Clement & Walker 1991; Clement & Shelton 1999) present various analyses of the known variables at their times of writing.

In the following sections, we describe the use of our time series Vi photometry to search for new variables and to revisit the identifications, periodicities and light curves of the known variables.

4.1 Search for variable stars

We have been guided in the identification of the known variables by the finding charts of Clement et al. (1984) and Clement & Shelton (1996) and by the equatorial coordinates of the variables in NGC 6333 given by Samus et al. (2009). We had no problems identifying

Table 3. General data for all of the confirmed variables in NGC 6333 in the FOV of our images. Stars V22–V34 are new discoveries in this work. Labels 'Bl' and 'd' are for Blazhko variables and double-mode RRd, respectively. The best previous period estimates for each variable from the Clement series of papers (Clement et al. 1984; Clement & Walker 1991; Clement & Shelton 1996, 1999) are reported in column 10 for comparison with our refined periods in column 7.

Variable star ID	Variable type	$\langle V \rangle$ (mag)	$\langle i \rangle$ (mag)	A_V (mag)	A_i (mag)	P (d) This work	β d Myr^{-1}	HJD$_{\max}$ (+245 0000)	P (d) Clement papers	RA (J2000.0)	Dec. (J2000.0)
V1	RRab	16.276	16.520	1.155	0.758	0.585 7309		5779.2366	0.585 728	17:19:18.32	−18:32:21.6
V2	RRab	16.209	16.391	1.110	0.683	0.628 1843		5665.4329	0.628 186	17:19:14.77	−18:31:36.2
V3	RRab-Bl	16.364	16.586	>1.00	>0.70	0.605 206		5664.4684	0.605 353	17:19:26.41	−18:34:34.8
V4	RRab	16.168	16.456	1.017	0.677	0.671 3000		5723.4130	0.671 3021	17:19:13.62	−18:31:39.6
V5	RRc	16.256	16.548	0.449	0.285	0.378 8136		5666.4490	0.378 812	17:19:14.36	−18:31:12.5
V6	RRab	16.351	16.478	1.000	0.672	0.606 7809		5666.4452	0.607 795	17:19:07.02	−18:31:20.9
V7	RRab	16.566	16.655	1.120	0.715	0.628 4626		5723.3838	0.628 4615	17:19:04.18	−18:32:24.4
V8	LPV	14.871	12.684	>0.69	>0.18	–		–	407	17:19:06.84	−18:32:42.8
V9	RRc	16.261	–	>0.38	–	0.322 9883		6166.5212	0.322 989	17:19:35.41	−18:34:17.1
V10	RRc-Bl	16.285	16.674	0.449	0.313	0.319 8454		6107.2557	0.319 820	17:19:14.53	−18:30:39.7
V11	RRab	16.065	16.300	0.704	0.543	0.742 4499		5723.4130	0.736 30	17:19:11.73	−18:31:14.8
V12	An.Cep	15.671	15.765	0.92	>0.51	1.340 255		5323.3075	1.340 204	17:18:52.69	−18:33:20.3
V13	RRab	17.681	17.963	1.183	0.780	0.479 8682		5323.3927	0.479 874	17:19:30.29	−18:30:54.6
V14	RRc	16.253	16.580	0.443	0.250	0.327 0530	4.67	5323.3708	0.326 91	17:19:14.14	−18:31:20.3
V15	RRab	16.239	16.343	0.971	0.760	0.641 7673		5723.4130	0.641 77	17:19:10.52	−18:29:59.2
V16	RRc-Bl?	16.073	16.569	0.336	0.218	0.384 6714		5724.3724	0.385 51	17:19:13.52	−18:30:43.0
V17	RRc	16.243	16.593	0.375	0.283	0.317 5888		5666.4294	0.317 59	17:19:10.48	−18:31:20.4
V18	RRc-Bl?	16.187	16.635	0.39	0.28	0.341 3440	11.50	5323.2745	0.342 28	17:19:10.61	−18:30:41.9
V19	RRd:	16.264	16.580	0.47	0.29	0.366 7937		5723.4130	0.366 48	17:19:12.76	−18:30:38.2
V20	RRc	16.340	16.591	0.423	0.219	0.314 1782		5323.2668	0.314 73	17:19:11.09	−18:31:02.7
V21	EW	16.818	16.884	0.30[b]	0.23[b]	0.720 4518		5724.3785	0.360 225	17:19:09.85	−18:32:34.5
V22	RRc-Bl	16.483	16.740	0.510	0.261	0.350 7561		5779.1641	–	17:19:03.12	−18:35:31.1
V23	RRc-Bl	16.513	16.827	0.311	0.178	0.304 6535		6108.1256	–	17:19:21.15	−18:30:10.2
V24	EW	17.381	17.520	0.45[b]	0.380[b]	0.366 784		6107.2525	–	17:19:13.04	−18:27:39.4
V25	E[c]	17.111	17.333	1.642[b]	1.330[b]	–		6107.2384[a]	–	17:19:25.94	−18:27:43.9
V26	LPV	17.380	17.066	>0.3	>0.18	–		–	–	17:19:13.84	−18:29:37.4
V27	LPV	17.069	16.625	>0.15	>0.2	–		–	–	17:18:56.40	−18:32:47.4
V28	LPV	13.216	12.413	>0.2	>0.15	–		–	–	17:19:11.68	−18:31:04.5
V29	LPV	13.591	–	>0.2	–	–		–	–	17:19:02.68	−18:32:53.6
V30	LPV	13.342	12.670	>0.1	>0.1	–		–	–	17:19:11.83	−18:31:27.9
V31	LPV	13.190	12.413	>0.15	>0.1	–		–	–	17:19:12.65	−18:31:01.7
V32	EW	15.961	–	0.19	–	0.172 30[d]		6162.6608	–	17:19:37.10	−18:35:40.1
V33	RRab	17.920	–	0.517	–	0.575 97		6164.5019	–	17:18:46.97	−18:25:29.5
V34	LPV	15.045	–	>0.1	–	–		–	–	17:18:45.62	−18:28:52.0

[a] Time of minimum light. [b] Depth of eclipse. [c] Possibly EA. [d] Real period may be twice this value.

all 21 known variables in our own time series data. Then, we applied a few approaches in the search for new variable star discoveries as we describe below.

First, we have defined a variability statistic $\mathcal{S}_{\mathcal{B}}$ as

$$\mathcal{S}_{\mathcal{B}} = \frac{1}{NM}\sum_{i=1}^{M}\left(\frac{r_{i,1}}{\sigma_{i,1}} + \frac{r_{i,2}}{\sigma_{i,2}} + \ldots + \frac{r_{i,k_i}}{\sigma_{i,k_i}}\right)^2, \quad (6)$$

where N is the total number of data points in the light curve and M is the number of groups of time-consecutive residuals of the same sign from the inverse-variance-weighted mean magnitude. The residuals $r_{i,1}$ to r_{i,k_i} form the ith group of k_i time-consecutive residuals of the same sign with corresponding uncertainties $\sigma_{i,1}$ to σ_{i,k_i}. Fig. 5 shows the distribution of the $\mathcal{S}_{\mathcal{B}}$ statistic as a function of mean magnitude for the 12 519 light curves for the stars in the Hanle V images.

This statistic, based on the original 'alarm' statistic $\mathcal{A}$ defined by Tamuz, Mazeh & North (2006), has been used by Arellano Ferro et al. (2012) to detect amplitude and period modulations in Blazhko variables. Its application to detecting light-curve variability was first introduced into our work by Figuera Jaimes et al. (2013), where we discuss in detail its application and how to set theoretical detection thresholds using simulated light curves.

As in Figuera Jaimes et al. (2013), we generated 10^5 simulated light curves for each star by randomly modifying the mean $\overline{V}$ magnitude within the uncertainty σ_i of each data point, i.e. $m_i = \overline{V} + \lambda_i\sigma_i$, where λ_i is a random deviate drawn from a normal distribution with zero mean and unit σ. Then, we used the resulting distribution of $\mathcal{S}_{\mathcal{B}}$ values to determine the 50 per cent and 99.9 per cent percentiles which we plot in Fig. 5 as the horizontal blue and red lines, respectively. Clearly the noise in the real Hanle V light curves is not Gaussian since many more than the expected ∼13 stars lie above the 99.9 per cent percentile for pure Gaussian noise. Furthermore, for stars brighter than ∼17.5 mag, the $\mathcal{S}_{\mathcal{B}}$ statistic increases with brightness in an exponential manner (linear in a logarithmic plot). All of these effects are due to residual systematic errors in the light curves that can mimic real variability. It is clear that our method of using simulated light curves to define the variability detection threshold has not worked very well for our Hanle V light curves of NGC 6333, contrary to what we found for the NGC 7492 light curves from Figuera Jaimes et al. (2013). This is because the $\mathcal{S}_{\mathcal{B}}$ statistic is especially sensitive to the systematic trends in the light

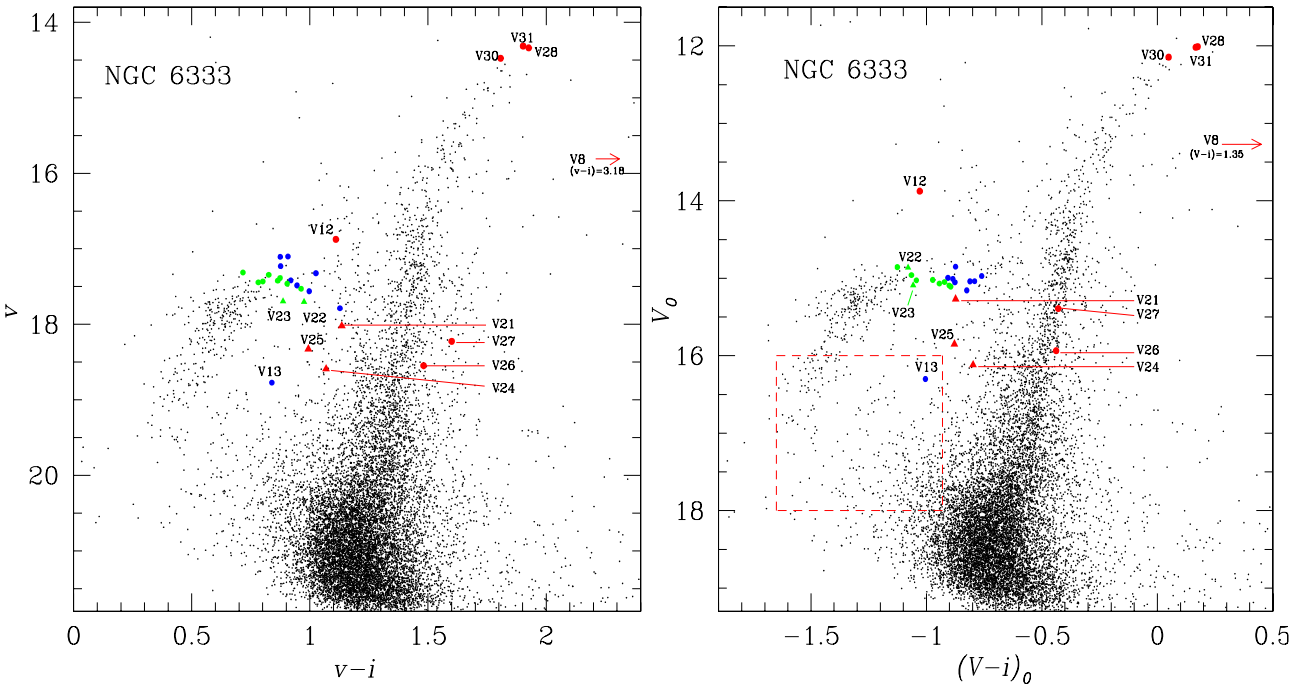

Figure 3. Colour–magnitude diagram of NGC 6333 for the Hanle data in the instrumental system (left) and after transforming v into the standard system and correcting for differential reddening (right) as described in the text. The coloured symbols correspond to the known variables and the new variables discovered in this paper. The colour coding is as follows: RRab stars – blue circles, known RRc stars – green circles, new RRc stars (V22, V23) – green triangles, long period variables (V8, V26, V27, V28, V30, V31) and AC (V12) – red circles, eclipsing binaries – red triangles. The region bounded by red dashed lines is an arbitrarily defined Blue Straggler region. New variables or interesting stars are discussed in Section 4.3 are labelled. The variables V29, V32, V33 and V34 are not plotted because they are either saturated in the I images, or outside the FOV of the Hanle data.

curves, and these trends are simply stronger and more coherent in the NGC 6333 light curves compared to the NGC 7492 light curves.

We therefore opted to define our variability detection threshold by eye as the dashed blue line in Fig. 5. All known variable stars in the FOV of our Hanle images lie above our chosen detection threshold by design. It is clear that the RR Lyrae stars have substantially larger values of $\mathcal{S}_{\mathcal{B}}$ among stars of their magnitude range. Long-term variables also stand clearly above the line. We explored the light curves of all of the other stars above the threshold and could identify seven clear new variables to which we assigned variable numbers; two RRc stars (V22 and V23), two eclipsing binaries (V24 and V25) and three long-period variables (V26, V27 and V28). Their classifications and interesting properties will be discussed in Section 4.3. Candidate variables in the Blue Straggler (BS) region (see caption of Fig. 5) were investigated individually but none showed convincing indications of variability. A similar plot as in Fig. 5 was constructed for our V data from La Silla with very similar results.

As a second strategy, we also applied the string-length method (Burke, Rolland & Boy 1970; Dworetsky 1983) to each light curve to determine the period and a normalized string-length statistic S_Q. In Fig. 6, we plot the minimum S_Q value for each light curve as a function of their corresponding CCD x-coordinate. The known variables are plotted with the coloured symbols as described in the caption. The horizontal blue line is not a statistically defined threshold but rather an upper limit, set by eye, that contains the majority of the known variables. Below this line we might expect to find previously undetected variables. In addition to the known variables, there are 10 other stars with S_Q values below the blue line and their light curves were thoroughly examined for variability. We found long-term variability for three of them, which we assign variable star names as V29, V30 and V31. We note that this method did not work for V27 but its variability was confirmed by the analysis described below.

Finally, a third approach we have followed to identify variables in the field of our images is by detecting PSF-like peaks in a stacked image built from the sum of the absolute valued difference images normalized by the standard deviation in each pixel as described by Bramich et al. (2011). This method allowed us to confirm the variability of all of the new variables discovered so far and to find the new variables V32, V33 and V34.

The previously known variables, along with all of the new discoveries, are listed in Table 3.

The combination of the three approaches described above lead us to believe that our search for variable stars with continuous variations (i.e. *not* eclipsing binaries etc.) is fairly complete down to $V \sim 19$ for amplitudes larger than 0.05 mag and periods between about 0.02 d and a few hundred days.

4.2 Period determination and refinement

To aid in the refinement of the periods of the known and newly discovered variables, we have combined our data with the V light-curve data from Clement & Shelton (1999). We have noticed small zero-point differences, of the order of a few hundreds of a magnitude, between the three sets of data which may be different from star to star. This is to be expected since, at least for DIA, the error in the reference flux affects all photometric measurements for a single star from the same data set in the same way, and the data for Hanle and La Silla each have a separate reference image with independently measured reference fluxes. Thus, for the period calculation we have

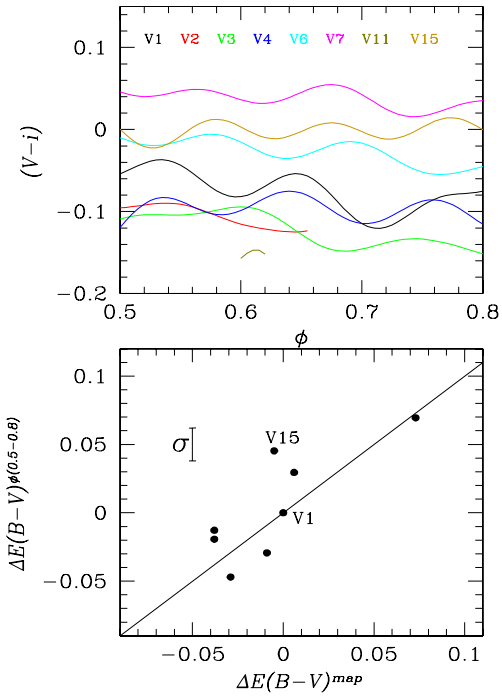

Figure 4. The top panel shows the difference between the Fourier fits to the standard V and instrumental i magnitudes for the light curves of the RRab stars in the phase interval 0.5–0.8. The different mean levels of these curves are due to the differential reddening affecting the cluster. V13 is not included in this analysis since it is not a cluster member (see Section 4.3). The Fourier fits of V2 and V11 are shown only in part since their light curves are not fully covered by data in the 0.5–0.8 phase range. In the bottom panel, we compare the differential values $\Delta E(B-V)^{\phi(0.5-0.8)}$ of a given variable relative to V1 with $\Delta E(B-V)^{\rm map}$ also relative to V1. The error bar represents the typical uncertainty in the colour differences.

proceeded as follows. First, the string-length method (Burke et al. 1970; Dworetsky 1983) was used to get a first estimate of the period. Then small magnitude shifts were applied as necessary to the light-curve data for each star so as to better align the data and a second string length was run on the levelled up light curve. The new period was used to phase the light curve and we explored for further magnitude shifts if any. Generally two to three iterations were sufficient to find an accurate period that phases the data precisely.

The new periods and those from the Clement series of papers are given in columns 7 and 10, respectively of Table 3. We note that in general the agreement is good but the new periods are considerably more precise. The light curves phased with the new periods are displayed in Figs. 7 and 8.

4.3 Individual stars

In this section, we discuss the nature of some interesting known variables and the newly discovered variable stars. To discuss their nature and cluster membership we have built the CMD of Fig. 3 by calculating the inverse-variance-weighted mean magnitudes of ∼11 800 stars that have both standard V and instrumental i magnitudes.

V3. This is an RRab star for which a strong evidence of exhibiting the Blazhko effect has been detected for the first time. Unfortunately our data do not fully cover the phased light curve at different amplitudes (see Fig. 7).

V5. Clement & Walker 1991 report this star as undergoing a period change. However, we do not detect this in our light curves combined with that from Clement & Shelton (1999), which have a combined baseline of ∼18 yr (see Fig. 8).

V8. This variable was announced by Sawyer (1951) as a long-period variable. A period of 407 d was suggested by Clement et al. (1984) and they commented on its small B amplitude of less than one magnitude. We show our light curves in V and i for this variable in Fig. 9. We are unable to estimate a period although the two observed minima are indeed separated by about 400 d. More data are required to complete the period analysis. The position of the star in the CMD is much to the red of the RGB, even in the CMD corrected for differential reddening, which implies that this star is not a cluster member. We note that the reddening required to bring this star back to the RGB if it is a cluster member is too large to be feasible for this field ($E(B-V) \approx 1.5$ mag).

V10. Clement & Walker 1991 also report this star as undergoing a period change as a period increase. Our light-curve data show small phase and amplitude variations reminiscent of the Blazhko effect in RRc stars (Arellano Ferro et al. 2012). Therefore, we believe that it is the Blazhko effect that has been detected previously and for which we present the first conclusive evidence of its presence in this star.

V12. The variability of this star was discovered by Sawyer (1951) who finds it of similar brightness to the RR Lyrae stars. Clement et al. (1984) classified it as a Population II (Pop II) Cepheid with a period of 1.340 204 d. They also find the star to be of similar B mag as the RR Lyrae stars which they use to argue that the star is either much obscured by the presence of a prominent cloud to the SW of the cluster or that it is not a cluster member. We confirm its periodicity as 1.340 255 d and we note that its position in the corrected CMD is about 1.05 mag brighter than the mean HB, suggesting that indeed it is likely to be a cluster member that suffers higher than usual extinction due to the obscuring cloud to the SW of the cluster (see Fig. 10). Clement et al. (2001) have pointed out that Cepheids tend to occur in globular clusters with blue HBs. Assuming that V12 is indeed a cluster member, and given the distance to the cluster (see Section 5.4), its absolute magnitude M_V is ∼−0.63 mag which along with its period, $\log P = 0.127$, places the star on the P–L relation for anomalous Cepheids (ACs) pulsating in the fundamental mode (Pritzl et al. 2002, see their fig. 6). ACs are more luminous than Pop II Cepheids for a given period, they have a similar colour to RRc stars but are 0.5–1.5 mag brighter, and their period can be between 0.5 and 3 d (Wallerstein & Cox 1984). V12 fulfils all of these characteristics, hence in the remainder of this paper we shall refer to V12 as an AC.

V13. This star was noted by Clement et al. (1984) to be much fainter than the other RR Lyrae stars in the cluster and they consider it to be a field star. This is a clear RRab star (see Fig. 7) and indeed it is ∼1.4 mag fainter than the other RRab stars. While NGC 6333 is known for having heavy differential reddening, we discard interstellar extinction as the cause of its faintness because its colour is similar to that of other RR Lyrae stars (Fig. 3). Hence, we agree with Clement et al. (1984) in arguing that V13 is not a member of the cluster but that instead it is a background object.

V14. The two periods 0.326 91 d from Clement & Shelton (1999) and 0.327 0659 d from the string-length method in this work fail to phase properly the combined light-curve data from Clement & Shelton (1999) and our light curves (Fig. 8). However, the period 0.327 0530 d accompanied with a secular period change rate of 4.67 d Myr^{-1} phases the light curve much better as it will be shown in Section 4.5.

Table 4. Fourier coefficients A_k for $k = 0, 1, 2, 3, 4$, and phases ϕ_{21}, ϕ_{31} and ϕ_{41}, for the nine RRab and seven RRc type variables for which the Fourier decomposition fit was successful. The numbers in parentheses indicate the uncertainty on the last decimal place. Also listed are the number of harmonics N used to fit the light curve of each variable, the deviation parameter $D_{\rm m}$ (see Section 5.1) and the colour excess $E(B-V)$.

Variable ID	A_0 (V mag)	A_1 (V mag)	A_2 (V mag)	A_3 (V mag)	A_4 (V mag)	ϕ_{21}	ϕ_{31}	ϕ_{41}	N	$D_{\rm m}$	$E(B-V)$ (mag)
					RRab stars						
V1	16.276(1)	0.401(1)	0.198(1)	0.141(1)	0.095(1)	3.910(8)	8.118(12)	6.109(16)	9	1.9	0.416
V2	16.209(1)	0.372(2)	0.187(2)	0.129(2)	0.093(2)	3.863(14)	8.167(22)	6.147(31)	9	2.4	0.378
V4	16.168(1)	0.341(1)	0.184(1)	0.119(1)	0.071(1)	4.124(11)	8.495(19)	6.664(27)	9	0.8	0.378
V6	16.351(1)	0.341(2)	0.175(2)	0.119(2)	0.079(2)	3.965(14)	8.194(21)	6.121(30)	9	2.7	0.422
V7	16.566(1)	0.379(1)	0.187(1)	0.130(1)	0.089(1)	3.941(9)	8.209(12)	6.226(17)	9	0.7	0.489
V11	16.065(1)	0.252(4)	0.129(4)	0.074(4)	0.031(4)	4.410(43)	8.903(67)	7.210(137)	7	4.9	0.387
V13	17.681(3)	0.403(4)	0.186(4)	0.139(4)	0.097(3)	3.804(31)	7.961(42)	5.870(64)	8	3.3	0.443
V15	16.239(3)	0.350(4)	0.186(4)	0.139(4)	0.074(4)	3.810(32)	8.060(49)	6.100(68)	8	3.7	0.411
V33	17.904(3)	0.212(5)	0.090(4)	0.025(4)	0.016(5)	4.407(75)	8.674(191)	7.929(271)	4	3.1	0.507
					RRc stars						
V5	16.256(1)	0.225(1)	0.028(1)	0.012(1)	0.008(1)	4.828(47)	3.932(105)	2.206(150)	4	–	0.388
V10	16.285(2)	0.232(3)	0.033(3)	0.013(3)	0.017(3)	5.013(87)	2.746(241)	1.390(164)	4	–	0.407
V14	16.253(2)	0.221(3)	0.048(3)	0.024(3)	0.021(3)	5.073(70)	3.241(126)	1.523(157)	4	–	0.382
V16	16.073(2)	0.188(2)	0.015(2)	0.025(2)	0.013(2)	3.919(137)	4.353(103)	1.580(157)	4	–	0.395
V17	16.243(2)	0.187(2)	0.044(2)	0.007(3)	0.016(2)	4.921(74)	3.894(400)	1.747(166)	4	–	0.403
V20	16.340 (1)	0.211(1)	0.036(2)	0.012(2)	0.001(1)	4.886(46)	2.967(123)	1.821(550)	4	–	0.396
V23	16.513(1)	0.149(2)	0.024(2)	0.007(2)	0.004(2)	4.891(73)	4.619(249)	2.684(294)	4	–	0.457

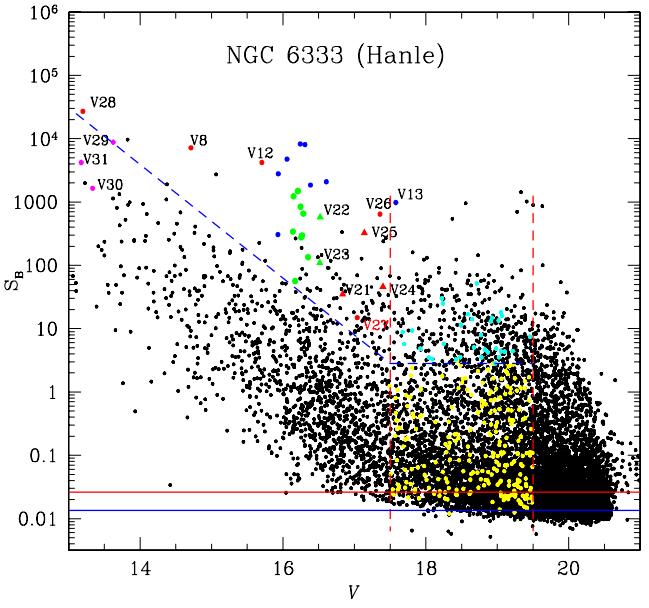

Figure 5. Distribution of the $\mathcal{S}_{\mathcal{B}}$ statistic as a function of mean V magnitude for 12 519 stars measured in the V Hanle images of NGC 6333. The coloured symbols for variable stars are as described in the caption of Fig. 3. Stars in the Blue Straggler region with $\mathcal{S}_{\mathcal{B}}$ below the variability detection threshold are plotted as yellow circles while cyan circles represent Blue Straggler stars with $\mathcal{S}_{\mathcal{B}}$ above the detection threshold and hence potential variable candidates of the SX Phe type. However, none of the Blue Stragglers was found to display convincing variability. The two vertical dashed red lines correspond to the magnitude limits set for the Blue Straggler region in the CMD.

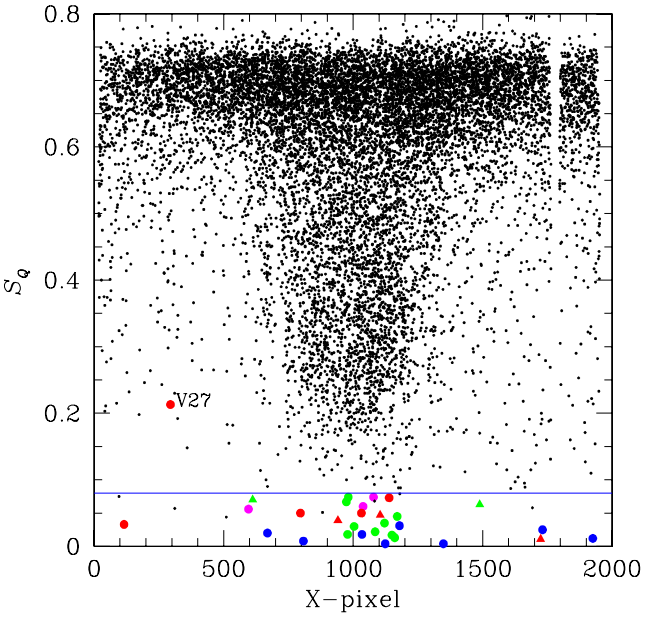

Figure 6. Minimum value of the string-length parameter S_Q calculated for the 12 519 stars with a light curve in our V reference image for the Hanle data, versus the CCD x-coordinate. The coloured symbols are as described in the caption of Fig. 3.

V16. Clement & Shelton (1996) speculate that this star is a double-mode RR Lyrae (RRd). However, we have been able to phase the three available sets of V data with one single period 0.384 6714 d, and we do not find any signs of secondary frequencies in the frequency spectrum. Thus, we do not confirm the double-mode nature of this RRc star (see discussion in Section 4.4) but the star may be a Blazhko variable (see Fig. 8).

V17. The light curve of this star can be seen in Fig. 8. We note that the celestial coordinates given by Samus et al. (2009) seem to point to the bright star near V17 while the authentic V17 is the more northern fainter star of the pair. The correct coordinates are given in Table 3 and a proper identification is in Fig. 10.

V18. The light curve of this RRc star displays nightly phase modulations which can be partially explained by a secular period change

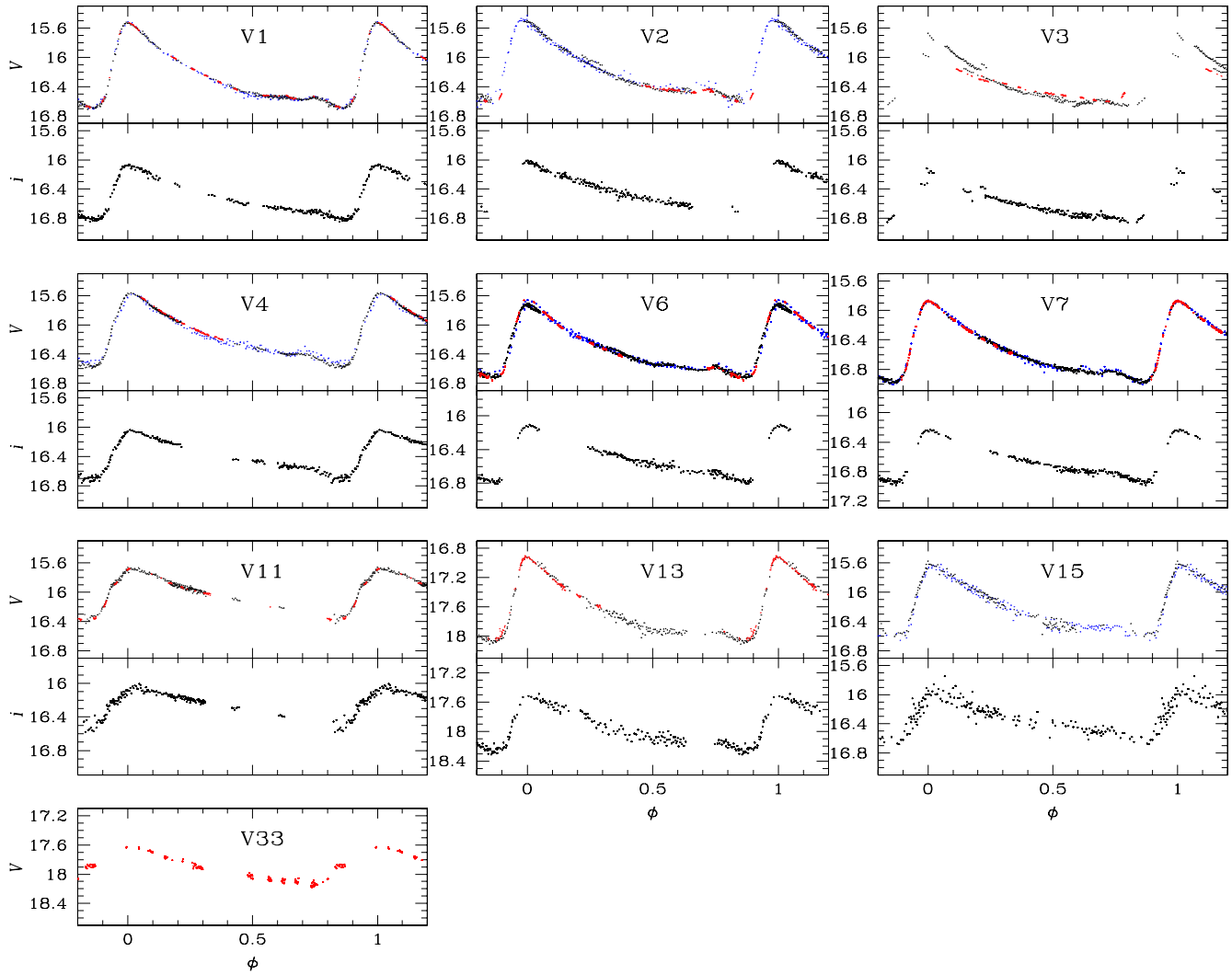

Figure 7. Standard V and instrumental i light curves of the RRab stars in NGC 6333 phased with the periods listed in Table 3. The blue points represent V data from Clement & Shelton (1999). The black and red points represent Hanle and La Silla data, respectively.

(see Section 4.5). However, some modulations remain suggesting the presence of the Blazhko effect. Unfortunately, its light curve is noisy due to the position of the star in a heavily crowded region.

V19. The light curve of this RR Lyrae star displays nightly phase modulations since its light curve is not cleanly phased with the period found by the string-length method (see Table 3). It also seems to show some very mild amplitude variations (Fig. 8). The light curve is also reminiscent of the RRc stars with Blazhko effect found in M53 by Arellano Ferro et al. (2012). In Section 4.4, we shall discuss the possible double-mode nature of V19.

V21. The variability of this star was discovered by Clement & Shelton (1996). These authors noticed that the star is fainter than the other RR Lyrae stars in the cluster and that it has a substantially different Fourier ϕ_{21} parameter. Hence, they concluded that it is either not an RR Lyrae star or that it is not a cluster member. Later, Clement in the CVSGC classify it as an EW variable. In the corrected CMD, the star falls just below the HB by ∼0.3 mag. Our best period is 0.720 4518 d and it produces the light curve of Fig. 11, where we notice two minima of different depths, typical of semi-contact binaries. Thus, we agree that the star is an EW star but with a period approximately double the one reported in Clement & Shelton (1996, 1999). The finding chart in Clement & Shelton (1996) is a bit misleading since the star is hardly visible in their map. This has probably led Samus (2009) to providing the wrong RA and Dec. which correspond to a neighbouring star. The correct coordinates are given in Table 3. The star is properly identified in our finding chart of Fig. 10.

V22 and V23. We have discovered these two new variables. Their period, light curves (see Fig. 8) and position in the CMD lead us to classify them as RRc stars. The light curve of V22 shows strong phase and amplitude modulations, while the light curve of V23 also shows phase and amplitude modulations to a lower level. We therefore conclude that both stars may exhibit the Blazhko effect. However, in Section 4.4 we shall explore the double-mode possibility by searching for a secondary frequency in the spectrum.

V24. This is a new eclipsing binary with a period of 0.366 784 d with two different eclipse depths (see Fig. 11). Its period along with its position in the corrected CMD ∼1.2 mag below the HB support its classification as a W Ursae Majoris-type binary (or EW).

V25. The light curve of this new eclipsing binary is shown in Fig. 12. One eclipse has been detected at HJD 245 6107.24 in both

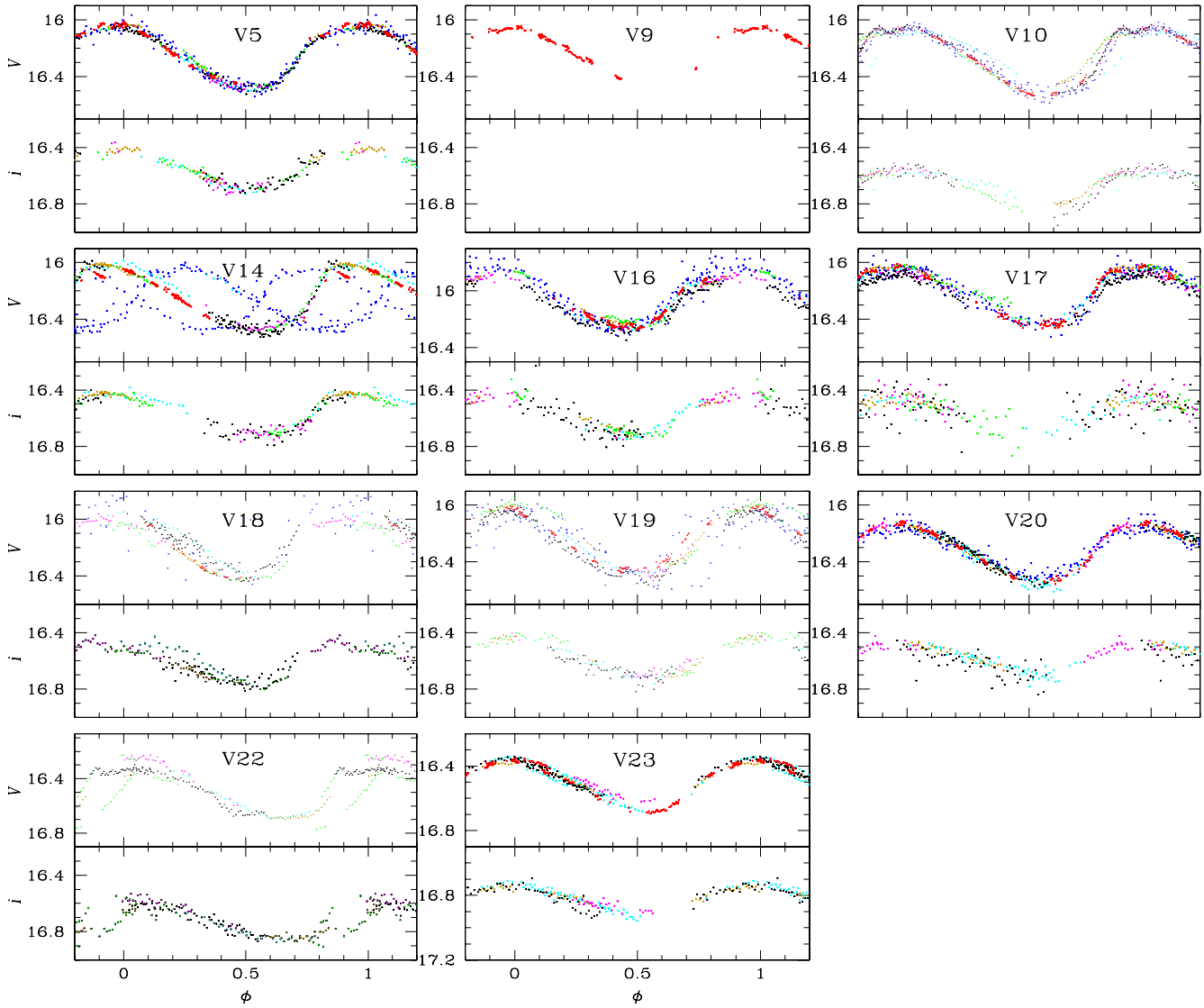

Figure 8. Standard V and instrumental i light curves of the RRc stars in NGC 6333 phased with the periods listed in Table 3. To highlight any phase and amplitude modulations, colours have been assigned for different observing runs: 1994 and 1995 May – blue (Clement & Shelton 1999), 2010 May – cyan, 2011 April – olive, 2011 June–August – green, 2012 May – purple, 2012 June – black, 2012 August – red. The variable V9 is outside of the FOV of the Hanle images and thus only its V light curve from the La Silla data is displayed. Note that the light curves for V14 and V18 have been phased with the best period determined without modelling a secular period change.

the V and I filters. With only one eclipse we are unable to estimate the orbital period. We note that there is also the hint of ellipsoidal variations in the out-of-eclipse light curve.

V26, V27, V28, V29, V30, V31 and V34. The light curves of these new variable stars show long-term variations (Fig 9). For V29 and V34, we have no I-band data. However, the rest of these variables are located well within the RGB in the CMD (Fig. 3). Our data are not sufficient to calculate their periods.

V32. The light curve of this new variable is shown in Fig. 13 phased with our best period found by the string-length method of 0.172 30 d. Twice this period would produce a clean double-wave light curve with some suggestion of different depth minima. The star is outside the FOV of our Hanle images and therefore we only have V-band data from La Silla. Although its mean magnitude $V \sim$ 16 mag is similar to the brightness of the RRc stars in the cluster, we believe the star is rather an eclipsing binary of the W Ursae Majoris-type (or EW), whose period and nature can be better defined upon obtaining further accurate data.

V33. The light curve phased with our best period 0.575 40 d is shown in Fig. 7. This new variable star is obviously an RRab star but given its mean magnitude $V \sim$17.94 mag it must be a field star further away than NGC 6333. The star is outside the FOV of our Hanle images.

V34. This new variable is a long-term pulsator whose variability is clear in the three nights of data as shown in Fig. 9. The star is outside the FOV of our Hanle images.

4.4 Double-mode pulsators

Clear phase and/or amplitude modulations are seen in several of the RRc light curves in Fig. 8. Phase and amplitude modulations can be the result of a Blazhko effect or a double-mode pulsation.

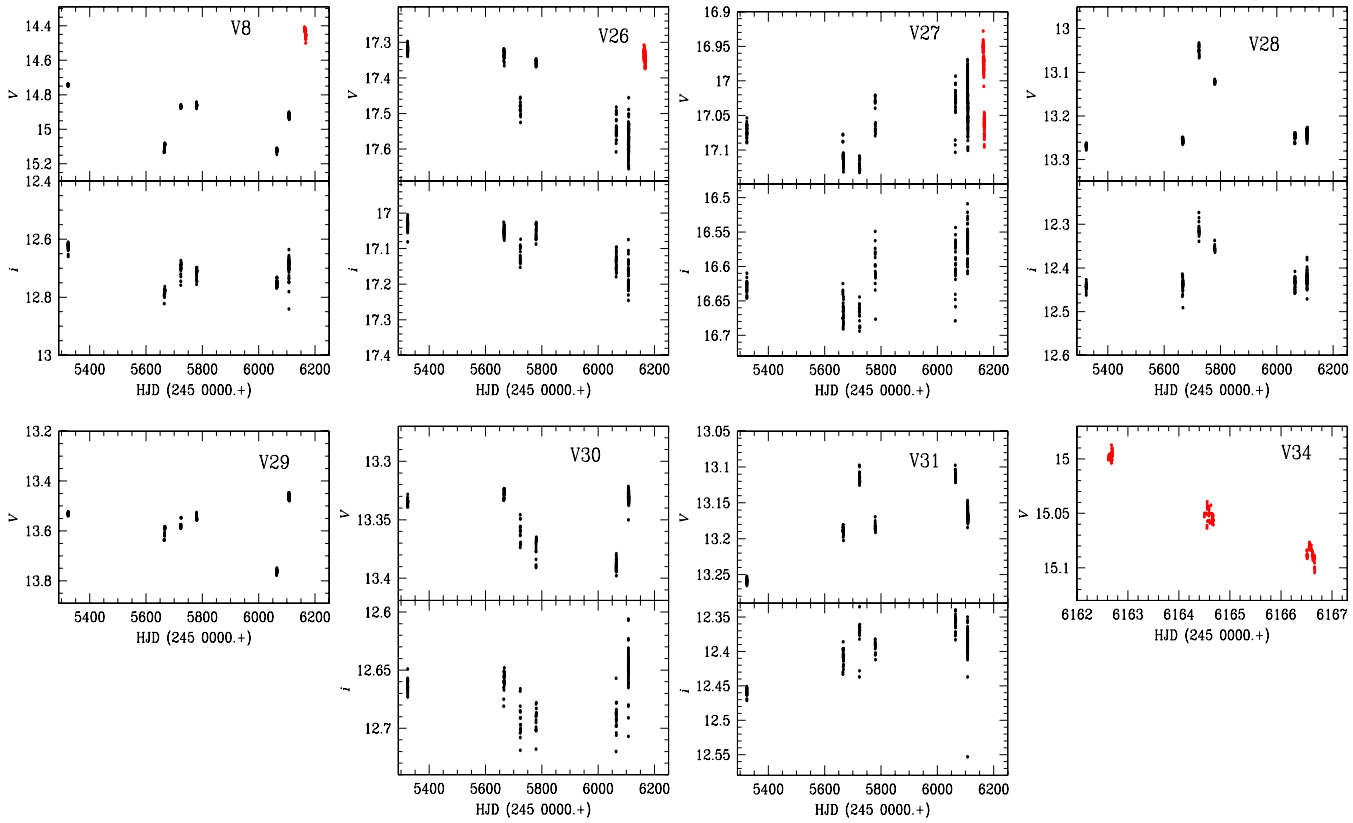

Figure 9. *V* and *i* magnitude variations of the LPVs in NGC 6333. The black and red symbols are data from Hanle and La Silla, respectively. V29 is saturated in our Hanle *I*-band images. V28, V29, V30 and V31 are saturated in our La Silla *V*-band images. V34 is outside the FOV of our Hanle images.

To distinguish between these possibilities one requires a convincing identification of secondary periods in the light curve and a long time series of accurate photometry is generally needed. Despite the limitations of our data set we have attempted the identification of such secondary periods for the RRc stars showing, to some extent, phase modulations, i.e. V10, V16, V18, V19, V22 and V23.

We used the program PERIOD04 (Lenz & Breger 2005) to identify the primary or first overtone period P_1 previously found by the string-length method described in Section 4.2 and given in column 7 of Table 3. Then, we pre-whitened the data from the primary period and searched the residuals for a secondary period. The frequency spectra of the original light curves and the residuals are shown in Fig. 14. No significant secondary frequencies were detected in the residual spectra of V10, V16, V18, V22 and V23 other than small residuals at the 1 d aliases of the main frequency f1. For V22 however, the amplitude modulations are so prominent that they could not be explained by period variations and rather they must be the result of the Blazhko effect whose periodicity we are not in position to estimate given our data set.

For V19, a rather prominent frequency was found in the residual spectrum at 2.029 49 d^{-1}, or a period of 0.492 734d. If this period is interpreted as the fundamental P_0 and with $P_1 = 0.366\ 7937$d we find a ratio $P_1/P_0 = 0.744$ which corresponds to the canonical 0.746 ± 0.001 ratio in RRd stars (Cox, Hudson & Clancy 1983; Catelan 2009) and with the period ratio found in a large sample of double-mode RRd stars in the Large Magellanic Cloud (LMC) (Alcock et al. 2000). P_0 produces a residuals light curve shown in Fig. 15. The above two facts strongly suggest that V19 is indeed a double-mode RR Lyrae or RRd star. An inspection of the light curve of V19 in fig. 4 b of Clement & Shelton (1996) reveals clear nightly phase drifts like those noted by these authors for V16; however, this case was not pursued further by them.

Thus, V10, V16, V18, V22 and V23 are rather reminiscent of the Blazhko RRc variables in NGC 5024 (Arellano Ferro et al. 2012). Given the nature of our time series we cannot estimate their Blazhko period or the possible presence of non-radial modes for which dense, accurate and prolonged observations are required as recent experience has shown in targets of space missions (e.g. Guggenberger et al. 2012, and references there in).

4.5 RRc stars with secular period variation

The RRc stars V14 and V18 show the largest phase variations not obviously accompanied with amplitude modulations. This is suggestive of a secular period change. To investigate this possibility, we have used a variation of the string-length method previously described in Bramich et al. (2011). We define

$$\phi(t) = \frac{t-E}{P(t)} - \left\lfloor \frac{t-E}{P(t)} \right\rfloor \tag{7}$$

$$P(t) = P_0 + \beta(t-E), \tag{8}$$

where ϕ(t) is the phase at time t, $P(t)$ is the period at time t, P_0 is the period at the epoch E and β is the rate of period change. We fix the value of E and calculate the best-fitting values of P_0 and β (in units d d^{-1}) within a small range of possible periods around the previously found best-fitting period as described in Section 4.2. We have applied this approach to the light curves of V14 and V18, both of which show clear phase displacements over time (see Section 4.3).

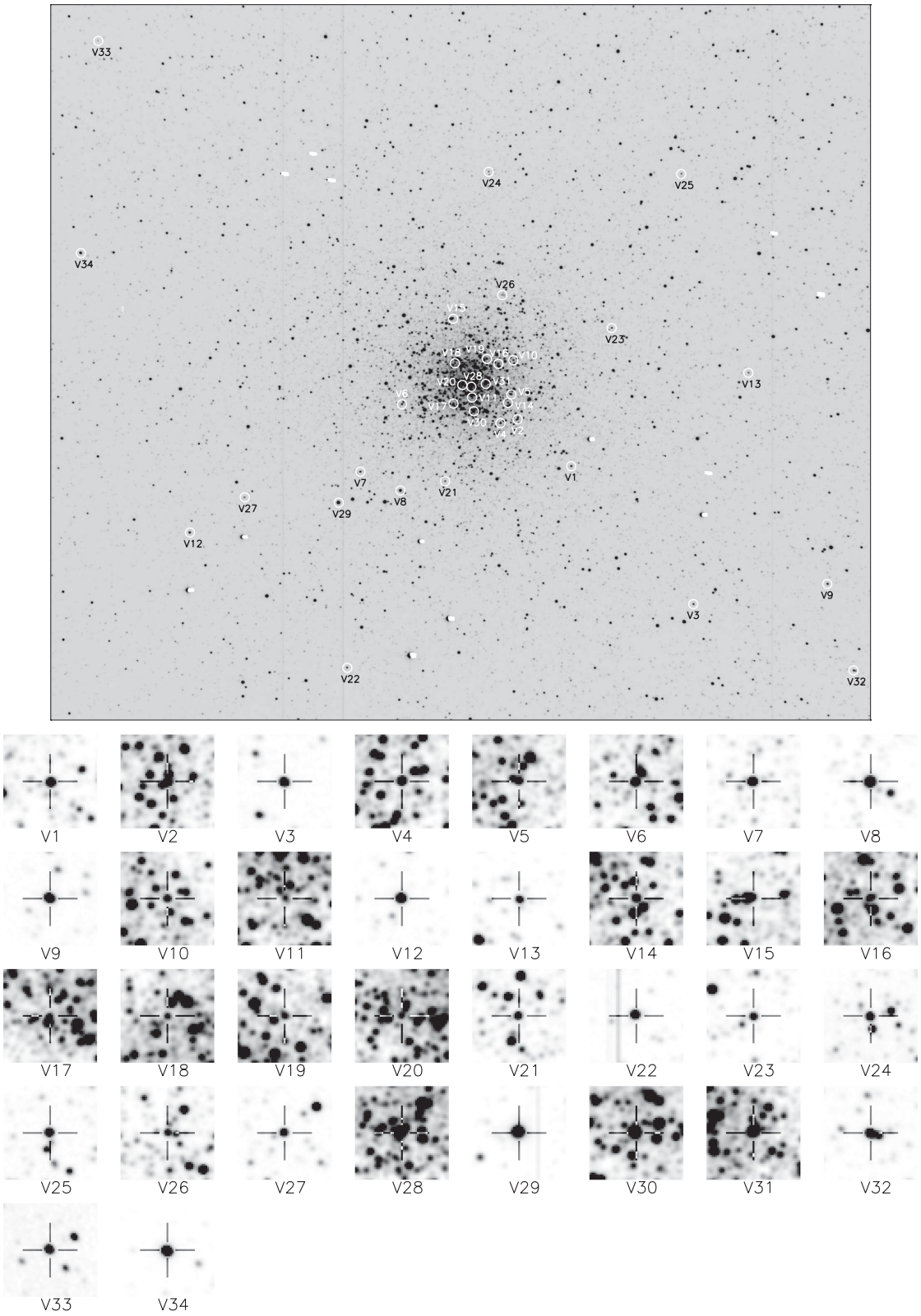

Figure 10. Finding charts constructed from our La Silla *V* reference image; north is up and east is to the right. The cluster image is 13.04 × 11.39 arcmin^2, and the image stamps are of size 20.6 × 20.6 arcsec^2. Each confirmed variable lies at the centre of its corresponding image stamp and is marked by a cross-hair.

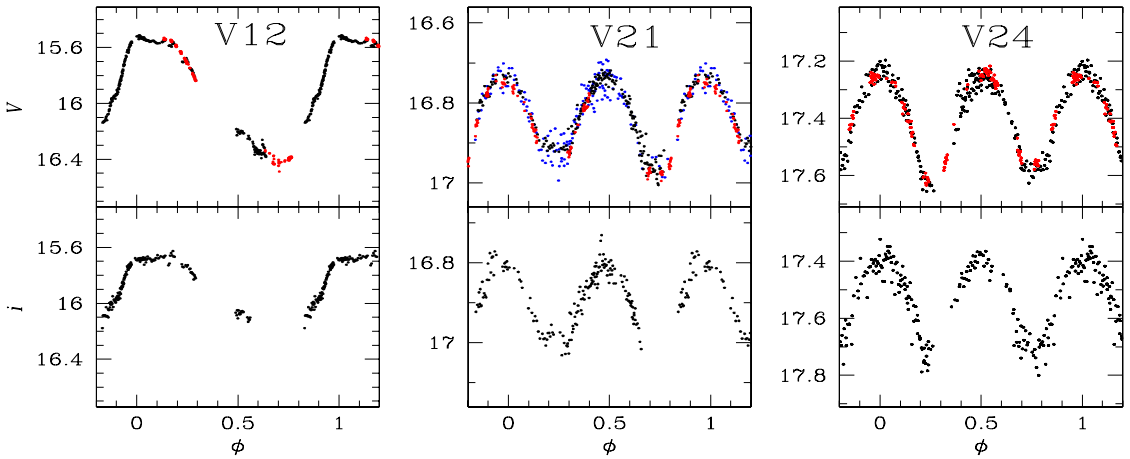

Figure 11. *V* and *i* light curves of the AC V12, and the eclipsing binaries V21 and V24, phased with the periods given in Table 3. The black and red points are data from Hanle and La Silla, respectively. The blue points correspond to the *V* observations of Clement & Shelton (1999).

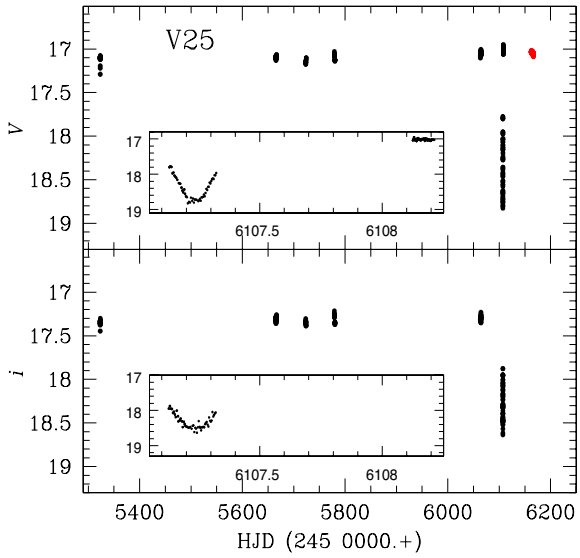

Figure 12. Light curve of V25 where one eclipse has been detected at HJD 245 6107.24d. The inset panel is a zoom-in on the eclipse. The black and red points represent Hanle and La Silla data, respectively.

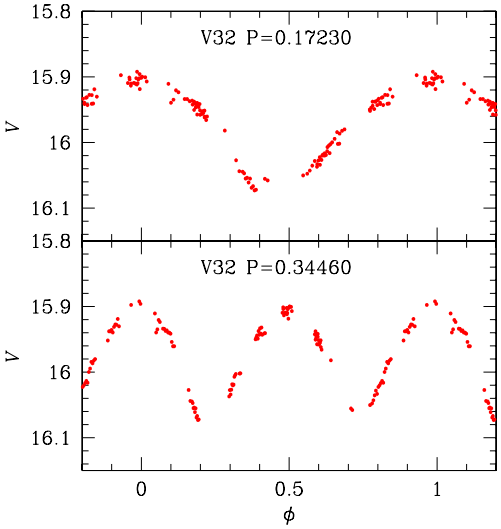

Figure 13. Light curve of the binary star V32 phased with two possible periods. The star is out the FOV of Hanle, hence we can only plot data from La Silla.

In Fig. 16, we show the light curves of these two stars phased with a constant period (top panels), and with the new period and period change rate calculated with the above equations (bottom panels). It is clear that the new periods and period change rates produce much cleaner and more coherent light curves. We conclude that V14 and V18 have secular period changes at the rates of 4.67 and 11.5 d Myr^{-1}, respectively. In the case of V18, the light curve phasing is still not fully satisfactory and therefore we do not discard the possibility of additional amplitude modulations that could be associated with a Blazhko effect similar to many of the RRc stars in NGC 5024 (Arellano Ferro et al. 2012).

4.6 Search for variable stars among the blue stragglers

The BS region in NGC 6333 is arbitrarily defined in Fig. 3 by the dashed red lines. In Fig. 5, this translates to the magnitude limits indicated by the two vertical red dashed lines. In this figure, all of the stars in the BS region are plotted with coloured points; yellow or cyan depending on whether they lie below or above the chosen variability detection threshold for $\mathcal{S}_{\mathcal{B}}$. We found that 40 of the BS stars have the $\mathcal{S}_{\mathcal{B}}$ statistic for the Hanle data above this threshold and their light curves were explored in detail. However, no clear and convincing variability was found in any of these stars and the relatively high value of $\mathcal{S}_{\mathcal{B}}$ could always be explained by groups of spurious photometric measurements or by the effect on the photometry of a nearby known variable. We conclude that if SX Phe stars exist in this cluster, then they must be of an amplitude similar to or smaller than the rms achieved by our photometry (see Fig. 2). To highlight this point, if we consider that the known SX Phe stars in NGC 5024 (another OoII cluster, with a blue HB and similar metallicity to NGC 6333) (Arellano Ferro et al. 2011) actually existed instead in NGC 6333, then we would have been able to detect about 19 out of 25(76 per cent) of them in our data, given the completeness of our variable star search reported at the end of Section 4.1.

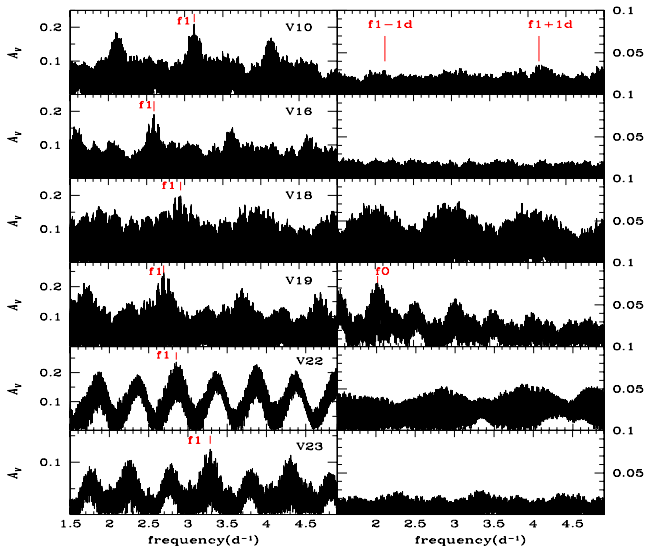

Figure 14. Frequency spectra of selected RRc stars. The left-hand panels show the spectrum produced by the original data. The major peaks correspond to the periods listed in Table 3 and used to produce the light curves in Figs 7 and 8. The right-hand panels show the spectra of the residuals after pre-whitening the main frequency. Note that the vertical scale in the right-hand panels has been increased to highlight possible secondary frequencies. See the text for a discussion.

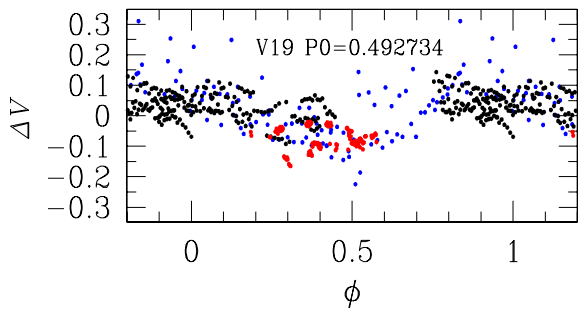

Figure 15. Residuals of V19 phased with the fundamental period given in the legend. The blue points are the V data from Clement & Shelton (1999). The black and red points are the V data from Hanle and La Silla, respectively. See Section 4.4 for a discussion.

5 RR Lyrae STARS

5.1 [Fe/H] and M_V from light-curve Fourier decomposition

Estimates of physical parameters, such as metallicity, luminosity and effective temperatures can be made from the Fourier decomposition of the light curves of RR Lyrae stars into their harmonics and from semi-empirical relationships (e.g. Jurcsik & Kovács 1996; Morgan, Wahl & Wieckhorts 2007). Traditionally the light curves are represented by the equation:

$$m(t) = A_o + \sum_{k=1}^{N} A_k \cos\left(\frac{2\pi}{P}k(t-E) + \phi_k\right), \qquad (9)$$

where $m(t)$ are magnitudes at time t, P the period and E the epoch. A linear minimization routine is used to fit the data with the Fourier series model, deriving the best-fitting values of the amplitudes A_k and phases ϕ_k of the sinusoidal components. From the amplitudes and phases of the harmonics in equation (9), the Fourier parameters

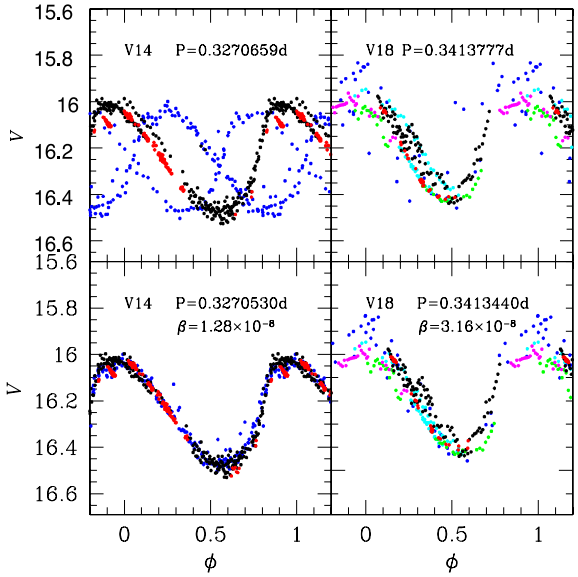

Figure 16. Two RRc stars with secular period change. The top panels show the light curves phased with a constant period found as described in Section 4.2. The bottom panels show the light curves phased with the new period and period change rate β given in the legend. The colours are coded as in the caption of Fig. 8.

$\phi_{ij} = j\phi_i - i\phi_j$ and $R_{ij} = A_i/A_j$ are defined. Although the V data from Clement & Shelton (1999) have been very useful in refining the periods of the RR Lyrae stars, in fitting the light curves we have opted not to include the data since they have a considerably larger scatter. The mean magnitudes A_0, and the Fourier light-curve fitting parameters of the individual RRab- and RRc-type stars in V are listed in Table 4.

The Fourier decomposition parameters can be used to calculate [Fe/H] and M_V for both RRab and RRc stars by means of the semi-empirical calibrations given in equations (10), (11), (12) and (13).

The calibrations for [Fe/H] and M_V used for RRab stars are

$$[\mathrm{Fe/H}]_J = -5.038 - 5.394P + 1.345\phi_{31}^{(s)}, \qquad (10)$$

$$M_V = -1.876\log P - 1.158A_1 + 0.821A_3 + K, \qquad (11)$$

given by Jurcsik & Kovács (1996) and Kovács & Walker (2001), respectively. The standard deviations of the above calibrations are 0.14 dex (Jurcsik 1998) and 0.04 mag, respectively. In equation (11), we have used $K = 0.41$ to scale the luminosities of the RRab with the distance modulus of 18.5 mag for the LMC (see the discussion in section 4.2 of Arellano Ferro, Giridhar & Bramich 2010). Equation (10) is applicable to RRab stars with a *deviation parameter* D_m, defined by Jurcsik & Kovács (1996) and Kovács & Kanbur (1998), not exceeding an upper limit. These authors suggest $D_m \leq 3.0$. The D_m is listed in column 11 of Table 4. A few stars have D_m marginally larger than this limit but given the quality of their light curve and the good coverage of the cycle we opted for reporting their iron abundance. The metallicity scale of equation (10) was transformed into the widely used scale of Zinn & West (1984) using the relation $[\mathrm{Fe/H}]_J = 1.431[\mathrm{Fe/H}]_{ZW} + 0.88$ (Jurcsik 1995). These two metallicity scales closely coincide for [Fe/H] ~ -2.0 while for [Fe/H]~ -1.5, the $[\mathrm{Fe/H}]_J$ is about 0.24 dex less metal poor than $[\mathrm{Fe/H}]_{ZW}$ (see also Fig. 2 of Jurcsik 1995). Therefore, for a metal poor cluster such as NGC 6333, the two scales are not significantly different.

Table 5. Physical parameters for the RRab and RRc stars. The numbers in parentheses indicate the uncertainty on the last decimal place and have been calculated as described in the text.

Star	[Fe/H]$_{ZW}$	M_V	log(L/L$_\odot$)	log $T_{\rm eff}$	M/M$_\odot$	R/R$_\odot$
			RRab stars			
V1	−1.666(11)	0.497(1)	1.701(1)	3.808(7)	0.73(6)	5.77(1)
V2	−1.780(21)	0.464(3)	1.714(1)	3.803(8)	0.73(7)	6.00(1)
V4	−1.634(18)	0.438(1)	1.725(1)	3.800(8)	0.70(6)	6.15(1)
V6	−1.674(20)	0.520(3)	1.692(1)	3.805(8)	0.70(6)	5.78(1)
V7	−1.742(11)	0.456(1)	1.717(1)	3.803(7)	0.73(6)	6.01(1)
V11	−1.519(63)	0.422(6)	1.731(2)	3.794(17)	0.66(13)	6.38(4)
V13[a]	−1.415(43)	0.656(6)	1.638(2)	3.819(10)	0.71(8)	5.09(2)
V15	−1.932(46)	0.456(6)	1.717(2)	3.798(10)	0.75(9)	6.14(2)
V33[a]	−1.107(181)	0.635(7)	1.646(3)	3.803(31)	0.68(25)	5.54(7)
Weighted mean	−1.702(6)	0.467(1)	1.713(1)	3.803(3)	0.72(3)	5.73(1)
			RRc stars			
V5	−1.81(22)	0.518(2)	1.693(1)	3.885(1)	0.49(1)	4.54(7)
V10	−1.83(44)	0.527(4)	1.689(2)	3.862(1)	0.59(1)	4.44(13)
V14	−1.69(24)	0.499(3)	1.700(1)	3.863(1)	0.58(1)	4.46(7)
V16	−1.65(23)	0.530(6)	1.688(3)	3.859(1)	0.46(1)	4.48(7)
V17	−1.22(78)	0.537(3)	1.685(1)	3.869(2)	0.54(2)	4.28(20)
V20	−1.69(22)	0.609(2)	1.656(1)	3.864(1)	0.54(1)	4.23(7)
V23	−0.45(50)[a]	0.604(3)	1.658(1)	3.875(1)	0.49(1)	4.02(11)
Weighted mean	−1.71(11)	0.554(1)	1.638(1)	3.862(1)	0.51(1)	4.79(4)

[a]Values not included in the average. V13 and V33 are not cluster members.

For the RRc stars we employ the calibrations:

$$[\mathrm{Fe/H}]_{\rm ZW} = 52.466P^2 - 30.075P + 0.131\phi_{31}^{(c)2} - 0.982\phi_{31}^{(c)} - 4.198\phi_{31}^{(c)}P + 2.424, \quad (12)$$

$$M_V = 1.061 - 0.961P - 0.044\phi_{21}^{(s)} - 4.447A_4, \quad (13)$$

given by Morgan et al. (2007) and Kovács (1998), respectively. The standard deviations of the above calibrations are 0.14 dex and 0.042 mag, respectively. For equation (13) the zero-point was reduced to 1.061 mag to make the luminosities of the RRc consistent with the distance modulus of 18.5 mag for the LMC (see discussions by Cacciari, Corwin & Carney 2005; Arellano Ferro et al. 2010). The original zero-point given by Kovács (1998) is 1.261.

In the above calibrations the phases are calculated either from series of sines or of cosines as indicated by the superscript. We transformed our cosine series phases into the sine ones where necessary via the relation $\phi_{jk}^{(s)} = \phi_{jk}^{(c)} - (j-k)\frac{\pi}{2}$.

The physical parameters for the RR Lyrae stars are reported in Table 5. We have not included the star V3 since it has prominent Blazhko modulations and V9 because our observations are not sufficient to cover the complete light curve. Despite the fact that most RRc stars show to some extent amplitude and/or phase modulations, in calculating mean parameters, we only excluded stars with extreme modulations; namely V18 and V22. V19 was also not considered given its double-mode nature. We also excluded V13 and V33 which are not cluster members. V14 was considered only after the light curve was phased with the period change rate included, i.e. the light curve in the bottom panel of Fig. 16. The inverse-variance-square-weighted means are also given in Table 5. The systematic error in the metallicity estimates is of the order of the scatter in the calibrations of equations (10) and (12), i.e. 0.14 dex. Thus, the metallicity obtained from the RRab and RRc stars is $[\mathrm{Fe/H}]_{\rm ZW} = -1.70 \pm 0.01$ which can be converted to the new scale defined by Carretta et al. (2009) using UVES spectra of RGB stars in globular clusters by $[\mathrm{Fe/H}]_{\rm UVES} = -0.413 + 0.130[\mathrm{Fe/H}]_{\rm ZW} - 0.356[\mathrm{Fe/H}]^2_{\rm ZW}$. We find $[\mathrm{Fe/H}]_{\rm UVES} = -1.67 \pm 0.01$. Clement & Shelton (1999) found, from the light-curve Fourier decomposition of V2, V4, V6 and V7, the average $[\mathrm{Fe/H}]_{\rm ZW} = -1.77 \pm 0.08$ in good agreement with our result.

To the best of our knowledge no iron abundance of NGC 6333 has been calculated from high resolution spectroscopy. The first calculation of $[\mathrm{Fe/H}]_{\rm ZW} = -1.81 \pm 0.15$ was made from integrated photometry in the Q_{39} index calibration by Zinn (1980) and reported by Harris (1996) (2010 edition) on the modern ZW scale, $[\mathrm{Fe/H}]_{\rm ZW} = -1.77$. The iron abundance of NGC 6333 has also been estimated by Costar & Smith (1988) from the Preston (1959) ΔS parameter estimated on V1 and V3. These authors calculated a [Fe/H] value of −1.93 and −1.45 for these two variables, respectively, for an average of −1.71. They used the ΔS–[Fe/H] calibration of Butler (1975). Had they used the calibration of Suntzeff, Kraft & Kinman (1994) for RRab stars or Jurcsik's (1995) or Fernley's et al. (1998) their average [Fe/H] would have been −1.72, −1.73 and −1.92, respectively. The value [Fe/H] = −1.72 is commonly cited in the literature on NGC 6333, most likely from the ΔS result. We have to note however that the ΔS values were obtained only on two RR Lyrae stars (V1 and V3) at a single phase and that the method is strongly phase dependent. We should also keep in mind that V3 is a clear Blazhko variable. Thus, despite the good numerical

agreement with our results we do not find the comparison of particular relevance, and believe that our result $[Fe/H]_{ZW} = -1.70 \pm 0.01$ is more solidly sustained.

The weighted mean M_V values for the RRab and RRc stars are 0.467 ± 0.001 and 0.554 ± 0.001 mag, respectively (see Table 5) and will be used in Section 5.4 to estimate the mean distance to the cluster after differential reddening is considered.

5.2 RR Lyrae luminosities and effective temperatures

The values of M_V in Table 5 were transformed into $\log L/L_\odot = -0.4(M_V - M_{bol}^\odot + BC)$. The bolometric correction was calculated using the formula $BC = 0.06\ [Fe/H]_{ZW} + 0.06$ given by Sandage & Cacciari (1990). We adopted the value $M_{bol}^\odot = 4.75$ mag.

The effective temperature T_{eff} can be estimated for RRab stars from the calibrations of Jurcsik (1998):

$$\log(T_{eff}) = 3.9291 - 0.1112(V-K)_o - 0.0032[Fe/H], \quad (14)$$

with

$$(V-K)_o = 1.585 + 1.257P - 0.273A_1 - 0.234\phi_{31}^{(s)} + 0.062\phi_{41}^{(s)}. \quad (15)$$

For the RRc stars the calibration of Simon & Clement (1993) can be used:

$$\log(T_{eff}) = 3.7746 - 0.1452\log(P) + 0.0056\phi_{31}^{(c)}. \quad (16)$$

The validity and caveats of the above calibrations have been discussed in several recent papers (Cacciari et al. 2005; Arellano Ferro et al. 2008, 2010; Bramich et al. 2011) and the reader is referred to them for the details. We list the obtained T_{eff} values for the RR Lyrae stars in NGC 6333 for comparison with similar work in other clusters.

5.3 RR Lyrae masses and radii

Once the period, luminosity and temperature are known for each RR Lyrae star, its mass and radius can be estimated from the equations: $\log M/M_\odot = 16.907 - 1.47\log P_F + 1.24\log(L/L_\odot) - 5.12\log T_{eff}$ (van Albada & Baker 1971) and $L = 4\pi R^2\sigma T^4$, respectively. The masses and radii are given in Table 5 in solar units.

5.4 Distance to NGC 6333 from the RR Lyrae stars

The weighted mean M_V, calculated for the RRab and RRc in Table 5 can be used to estimate the true distance modulus; $V - M_V = 5\log d - 5 + 3.1E(B-V)$. The individual colour excesses are listed in Table 4 which were calculated after differential reddening was considered (Section 3). Although the internal errors in M_V are small, given the mean magnitude dispersion in the HB, a better estimate of the uncertainty in the distance is the standard deviation of the mean and so we find the distance modulus of 14.527 ± 0.052 mag and 14.482 ± 0.081 mag using the RRab and RRc stars, respectively, which correspond to the distances 8.04 ± 0.19 and 7.88 ± 0.30 kpc.

The above distances for the RRab and RRc stars are calculated from independent empirical calibrations, with their own systematic uncertainties, hence they should be considered as two independent estimates. The correction for differential reddening has contributed to the good agreement between these two estimates of the distance and to reduce the uncertainties.

The distance to NGC 6333 listed in the catalogue of Harris (1996) (2010 edition) is 7.9 kpc, estimated from the mean M_V magnitudes calculated by Clement & Shelton (1999). The calibrations of M_V used by Clement & Shelton for the RRab and RRc stars are the same as our equations (11) and (13) but before correcting the zero-points as discussed in Section 5.1. Also, in their calculation of the distance the differential reddening was not taken into account. These facts may account for the small difference in the distance we derive for the cluster.

The most recent discussion on the distance of the cluster is perhaps the one given by Casetti-Dinescu et al. (2010) in which they adopt the distance 7.9 kpc from Harris (1996) (2010 edition) but argue that due to reasonable uncertainties in the distance(10 per cent) the alternative distance of 8.6 kpc is selected such that it places the cluster on the opposite side of the Galactic centre. In our opinion and given our results, 10 per cent is large for a distance error and note that if our distance is adopted then the cluster would be located on the near side of the Galactic centre.

6 BAILEY DIAGRAM AND OOSTERHOFF TYPE

Using the periods listed in Table 3, we calculate mean periods of 0.639 and 0.336 d for the 8 RRab and 10 RRc stars, respectively, that are cluster members (i.e. excluding V13 and V33), and excluding the RRd star V19. These values clearly identify NGC 6333 as an Oosterhoff-type II (OoII) cluster.

The Bailey diagram ($\log P$ versus A_V and $\log P$ versus A_i) for the RR Lyrae variables is shown in Fig. 17. The RRab stars have longer periods for a given amplitude than their counterparts in the OoI cluster M3. This is also seen in the OoII clusters M53 (Arellano Ferro et al. 2011), M15 and M68 (Cacciari et al. 2005). This fact confirms the OoII type of NGC 6333. V13 and V33 are discordant stars and this supports the idea that they are not cluster members (Clement et al. 1984, Section 4.3). Other than V13 and V33 there are no RRab stars with peculiar amplitude, which gives support to the physical parameters obtained in Section 5 from the light-curve Fourier decomposition. The RRc stars show some scatter which is likely due to the amplitude modulations observed in the population of RRc stars in NGC 6333, the majority of the RRc stars seem to show some amplitude and/or phase modulations that can be attributed to the Blazhko effect (see Section 4.3 and Fig. 8). A similar case was found in NGC 5024 which probably contains the largest sample of RRc Blazhko variables (Arellano Ferro et al. 2011, 2012).

As in Arellano Ferro et al. (2011) for NGC 5024, in the bottom panel of Fig. 17 we show the Bailey diagram using the amplitudes in the I band, or A_i in Table 3, for NGC 6333. The solid curve is the fit calculated by Arellano Ferro et al. for the RRab stars in NGC 5024 (their equation 3). Being the two clusters of the OoII type and of similar metallicity, the match is rewarding.

7 CONCLUSIONS

In their analysis on the completeness of the variable stars sample in NGC 6333, Clement & Shelton (1996) concluded that the discovery of new RRc stars was unlikely but that some RRab stars might have escaped their attention. In fact, we have not found any new RR Lyrae, neither RRab nor RRc, in the corresponding field of Clement & Shelton's images. However, we found in this work two RRc stars, V22 and V23, and one RRab, V33; the three of them are relatively isolated in the outskirts of the cluster. While V22 and V23 are clear members of NGC 6333, V33 is a field RRab further away than the cluster. Likewise we corroborate that the RRab star V13

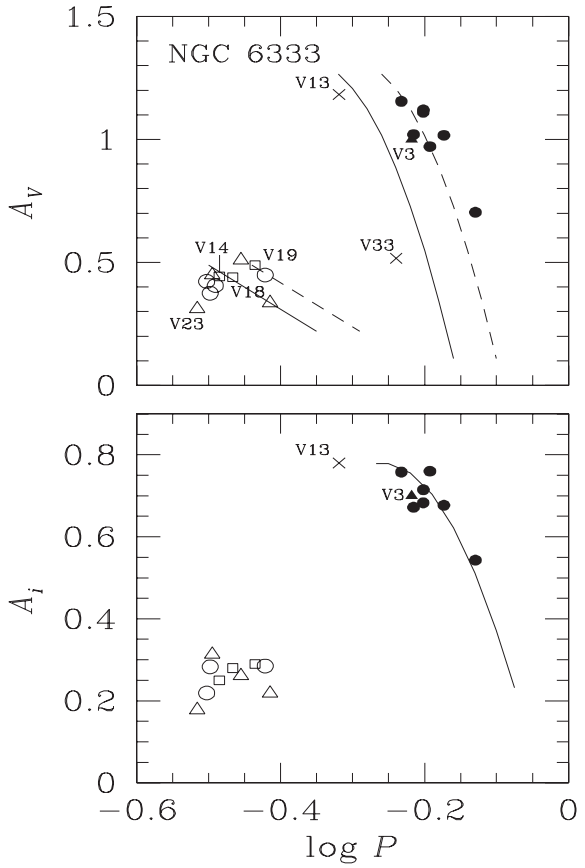

Figure 17. The RR Lyrae stars in NGC 6333 on the amplitude–period plane or Bailey diagram for the *V* and *I* bands. In the top panel, the solid lines represent the average distributions of fundamental and first overtone RRL's in M3. The segmented lines are the loci for the evolved stars according to Cacciari et al. (2005). The filled symbols are used for RRab stars and open symbols for RRc stars. Circles represent stars with no apparent signs of amplitude modulations and triangles indicate stars with clear and prominent amplitude modulations or Blazhko variables. Variables with secular period change, V14 and V18 and the double-mode star V19 are shown as squares. V13 and V33 are not cluster members. The bottom panel shows the case for the *I* amplitudes. The solid curve is the locus defined by Arellano Ferro et al. (2011) for the RRab stars in the OoII cluster NGC 5024.

is not a cluster member. We have also been able to find three new eclipsing binaries and seven long-period variables. Pulsation period refinements have been calculated for nearly all variables. Accurate celestial coordinates and a finding chart for all previously known and new variables are provided.

Although a cluster membership confirmation from radial velocity data would be necessary, we argue that V12 is a cluster member since the correction from interstellar reddening places this star in the Cepheid instability strip at about 1 mag above the HB. Although V12 is about 5 arcmin away from the cluster centre, it has been noted by Clement et al. (2001) in the CVSGC (2012 update) that the star is within the tidal radius of NGC 6333 of ∼8 arcmin. V12 also follows the *P–L* relation of ACs pulsating in the fundamental mode of Pritzl et al. (2002). While ACs are common in dwarf spheroidal galaxies (e.g. Nemec, Nemec & Lutz 1994; Pritzl et al. 2002, 2005), they are rare in globular clusters; only four are presently known, V19 in NGC 5466 (Zinn & Dahn 1976) and three in ω Cen (Kaluzny et al. 1997). We argue that V12 in NGC 6333 is an AC.

Among the RR Lyrae stars, we have identified the double-mode or RRd nature of V19 and the secular period changes in V14 and V18 at the rates of 4.67 and 11.5 d Myr^{-1}, respectively. We stress that similar to NGC 5024 (Arellano Ferro et al. 2012), NGC 6333 has a rather large number of Blazhko stars among the RRc population.

A deep search for variability among the BSs in the cluster was conducted but none was found. If SX Phe stars do exist in the cluster they must be of amplitudes smaller than the detection limit of our data.

The Fourier decomposition of the light curves of nine RRab and seven RRc stars was performed and individual values of [Fe/H], M_V, $\log L/L_\odot$, $T_{\rm eff}$ and stellar mass and radius were calculated using ad hoc semi-empirical calibrations. The weighted mean values of the iron abundance of selected stars gives a cluster mean metallicity of $[{\rm Fe/H}]_{\rm ZW} = -1.70 \pm 0.01$ in the Zinn & West (1984) scale or $[{\rm Fe/H}]_{\rm UVES} = -1.67 \pm 0.01$ in the scale defined more recently by Carretta et al. (2009). The weighted mean values of the absolute magnitude of the RRab and the RRc stars lead to a distance of 8.04 ± 0.19 and 7.88 ± 0.30 kpc, respectively. In calculating these distances the heavy differential reddening affecting the cluster was taken into account by using the detailed reddening map of Alonso-García et al. (2012).

ACKNOWLEDGEMENTS

We acknowledge an anonymous referee for very relevant input and comments. We are grateful to the TAC's of the Hanle and La Silla observatories for generous telescope time allocation to this project and to the support astronomers of IAO, at Hanle and CREST (Hosakote) for their very efficient help while acquiring the data. This project was supported by DGAPA-UNAM grant through project IN104612 and by the INDO-MEXICAN collaborative programme by DST-CONACyT. NK acknowledges an ESO Fellowship. The research leading to these results has received funding from the European Community's Seventh Framework Programme (/FP7/2007-2013/) under grant agreement No 229517. OW (aspirant FRS - FNRS), AE, YD, DR (FRIA PhD student), and J. Surdej acknowledge support from the Communauté française de Belgique – Actions de recherche concertées – Académie universitaire Wallonie-Europe. TCH gratefully acknowledges financial support from the Korea Research Council for Fundamental Science and Technology (KRCF) through the Young Research Scientist Fellowship Program. TCH acknowledges financial support from Korea Astronomy and Space Science Institute (KASI) grant number 2012-1-410-02. KA, DB, MD, MH and CL are supported by NPRP grant NPRP-09-476-1-78 from the Qatar National Research Fund (a member of Qatar Foundation). MR acknowledges support from FONDECYT postdoctoral fellowship N3120097. The Danish 1.54 m telescope is operated based on a grant from the Danish Natural Science Foundation (FNU). Funding for the Centre for Star and Planet Formation is provided by the Danish National Research Foundation. CS received funding from the European Union's Seventh Framework Programme (FP7/2007-2013) under grant agreement no. 268421. HK acknowledges support from a Marie-Curie Intra-European Fellowship.

This work has made a large use of the SIMBAD and ADS services.

REFERENCES

Alcock C. et al., 2000, ApJ, 542, 257

Alonso-García J., Mateo M., Sen B., Banerjee M., Catelan M., Minniti D., von Braun K., 2012, AJ, 143, 70

Arellano Ferro A., Rojas López V., Giridhar S., Bramich D. M., 2008, MNRAS, 384, 1444
Arellano Ferro A., Giridhar S., Bramich D. M., 2010, MNRAS, 402, 226
Arellano Ferro A., Figuera Jaimes R., Giridhar S., Bramich D. M., Hernández Santisteban J. V., Kuppuswamy K., 2011, MNRAS, 416, 2265
Arellano Ferro A., Bramich D. M., Figuera Jaimes R., Giridhar S., Kuppuswamy K., 2012, MNRAS, 420, 1333
Blanco V. M., 1992, AJ, 104, 734
Bramich D. M., 2008, MNRAS, 386, L77
Bramich D. M., Freudling W., 2012, MNRAS, 424, 1584
Bramich D. M., Figuera Jaimes R., Giridhar S., Arellano Ferro A., 2011, MNRAS, 413, 1275
Bramich D. M. et al., 2013, MNRAS, 428, 2275
Burke E. W., Rolland W. W., Boy W. R., 1970, J. R. Astron. Soc. Can., 64, 353
Butler D., 1975, ApJ, 200, 68
Cacciari C., Corwin T. M., Carney B. W., 2005, AJ, 129, 267
Cardelli J. A., Clayton G. C., Mathis J. S., 1989, ApJ, 345, 245
Carretta E., Bragaglia A., Gratton R., DOrazi V., Lucatello S., 2009, A&A, 508, 695
Casetti-Dinescu D. I., Girard T. M., Korchagin V. I., van Altena W. F., López C. E., 2010, AJ, 140, 1282
Catelan M., 2009, Ap&SS, 320, 261
Clement C. M., Shelton I., 1996, AJ, 112, 618
Clement C. M., Shelton I., 1999, AJ, 118, 453
Clement C. M., Walker I. R., 1991, AJ, 101, 1352
Clement C. M., Ip P., Robert N., 1984, AJ, 89, 1707
Clement C. M. et al., 2001, AJ, 122, 2587
Costar D., Smith H. A., 1988, AJ, 96, 1925
Cox A. N., Hudson S. W., Clancy S. P., 1983, ApJ, 266, 94
Draper P. W., 2000, in Manset N., Veillet C., Crabtree D., eds. ASP Conf. Ser. Vol. 216, Astronomical Data Analysis Software and Systems IX. Astron. Soc. Pac., San Francisco, p. 615
Dworetsky M. M., 1983, MNRAS, 203, 917
Fernley J., Skillen I., Carney B. W., Cacciari C., Janes K., 1998, A&A, 330, 515
Figuera Jaimes R., Arellano Ferro A., Bramich D. M., Giridhar S., 2013, A&A, in press (arXiv1305.4837)
Guggenberger E. et al., 2012, MNRAS, 424, 649
Guldenschuh K. A. et al., 2005, PASP, 117, 721
Harris W. E., 1996, AJ, 112, 1487
Honeycutt R. K., 1992, PASP, 104, 435
Jurcsik J., 1995, Acta Astron, 45, 653
Jurcsik J., 1998, A&A, 333, 571
Jurcsik J., Kovács G., 1996, A&A, 312, 111
Kains N., Bramich D. M., Figuera Jaimes R., Arellano Ferro A., Giridhar S., Kuppuswamy K., 2012, A&A, 548, 92
Kaluzny J., Kubiak M., Szymański, Udalski A., Krzemiński W., Mateo M., 1997, A&AS, 125, 343
Kovács G., 1998, Mem. Soc. Astron. Ital. 69, 49
Kovács G., Kanbur S. M., 1998, MNRAS, 295, 834
Kovács G., Walker A. R., 2001, A&A, 371, 579
Kunder A., Chaboyer B., Layden A., 2010, AJ, 139, 415
Lenz P., Breger M., 2005, Commun. Asteroseismol., 146, 53
Mateo M., Udalski A., Szymanski M., Kaluzny J., Kubiak M., Krzeminski W., 1995, AJ, 109, 588
Morgan S., Wahl J. N., Wieckhorts R. M., 2007, MNRAS, 374, 1421
Nemec J. M., Nemec A. F. L., Lutz T. E., 1994, AJ, 108, 222
Padmanabhan N. et al., 2008, ApJ, 674, 1217
Preston G. W., 1959, ApJ, 130, 507
Pritzl B. J., Armandroff T. E., Jacoby G. H., Da Costa G. S., 2002, AJ, 124, 1464
Pritzl B. J., Armandroff T. E., Jacoby G. H., Da Costa G. S., 2005, AJ, 129, 2232
Reed B. C., Hesser J. E., Shawl S. J., 1988, PASP, 100, 545
Regnault N. et al., 2009, A&A, 506, 999
Safonova M., Stalin C. S., 2011, AJ, 142, 179
Samus N. N., Kazarovets E. V., Pastukhova E. N., Tsvetkova T. M., Durlevich O. V., 2009, PASP, 121, 1378
Sandage A., Cacciari C., 1990, ApJ, 350, 645
Sawyer H. B., 1951, Pub. DDO, 1, 511
Schlegel D. J., Finkbeiner D. P., Davis M., 1998, ApJ, 500, 525
Shapley H., 1916, PASP, 28, 282
Simon N. R., Clement C. M., 1993, ApJ, 410, 526
Sturch C., 1966, ApJ, 143, 774
Suntzeff N. B., Kraft R. P., Kinman T. D., 1994, ApJS, 93, 271
Tamuz O., Mazeh T., North P., 2006, MNRAS, 367, 1521
van Albada T. S., Baker N., 1971, ApJ, 169, 311
Wallerstein G., Cox A. N., 1984, PASP, 96, 677
Zacharias N. et al., 2010, AJ, 139, 2184
Zinn R., 1980, ApJS, 42, 19
Zinn R., 1985, ApJ, 293, 424
Zinn R., Dahn C. C., 1976, AJ, 81, 527
Zinn R., West M. J., 1984, ApJS, 55, 45

SUPPORTING INFORMATION

Additional Supporting Information may be found in the online version of this article:

Table 2. Time-series *V* and *i* photometry for all the confirmed variables in our FOV (http://mnras.oxfordjournals.org/lookup/suppl/doi:10.1093/mnras/stt1080/-/DC1).

Please note: Oxford University Press is not responsible for the content or functionality of any supporting materials supplied by the authors. Any queries (other than missing material) should be directed to the corresponding author for the Paper.

This paper has been typeset from a TEX/LATEX file prepared by the author.